Faculty of Science

Slope Stability Analysis of Hamnbanan, Gothenburg

Andreas Thörn

Degree of Bachelor of Science
with a major in Earth Sciences
15 hec

Department of Earth Sciences
University of Gothenburg
2022 B-1208

UNIVERSITY OF GOTHENBURG

UNIVERSITY OF GOTHENBURG
Department of Earth Sciences
Geovetarcentrum/Earth Science Centre

Slope Stability Analysis of Hamnbanan, Gothenburg

Andreas Thörn

ISSN 1400-3821

B1208
Bachelor of Science thesis
Göteborg 2022

Mailing address
Geovetarcentrum
S 405 30 Göteborg

Address
Geovetarcentrum
Guldhedsgatan 5A

Telephone
031-786 19 56

Geovetarcentrum
Göteborg University
S-405 30 Göteborg
SWEDEN

Abstract

When constructing the new railroad link, Hamnbanan, between Eriksberg and Pölsebo more rock than anticipated fell out as wedges. Due to the excess amount of rock that had to be processed and shipped away there was an increase in cost. The purpose of this study is to see if the data available before rock blasting begun was sufficient to be able to avoid the extra volume of rock that had to be taken care of. By analysing discontinuities' orientations and characteristics it is possible to predict the factor of safety and probability of failure for a rock slope. These analyses were performed in software's from rocscience, and the findings show clear indications of steeper slope angles result in more volume of rock falling out.

Contents

1 Introduction

1.1 Hamnbanan

Hamnbanan is an extension of the railroad to the port of Gothenburg, the construction started in 2018 and the railway is scheduled to open in 2023. The development was ordered by the Swedish Transport Administration (Trafikverket) and executed by Skanska. The construction includes a new route through an approximately 1,1km long tunnel and an expansion from single track to double track. This is done so that more trains will be able to operate the route which will lead to more goods transferred from road-borne trucks to freight trains. Transportation on railroad is sustainable and the mode of transport that is most efficient from an environmental and economic perspective is the combination of cargo ships and trains. The port of Gothenburg is the largest in northern Europe with 65% of Sweden's freight containers and 30% of the country's foreign trade going through. A freight train can substitute 30 trucks, consequently this will decrease the number of trucks significantly and be beneficial both to the environment and by reducing traffic congestion (Trafikverket, 2022).

When construction of the railroad commenced large quantities of rock had to be removed and rock slopes where fabricated on either side of the NE-SW striking rail. When constructing rock slopes, it comes with a risk of loose wedges and/or blocks that can fail and fall out, in most cases companies will strive to avoid this e.g., by either bolting the loose blocks or by choosing a different slope dip.

1.2 Fundamentals of slope design and stability analysis

A critical factor of stability analysis is to estimate the strength of the rock mass and the discontinuities which control sliding. Constructed slopes requires an ongoing assessment of the stability of these slopes. The assessment depends on good geological, geotechnical and groundwater models as well as an understanding of the risks and economic consequences of slope instability. A good slope design incorporates all of these parameters to produce a balanced compromise between safety and operational/economic efficiency (Hoek, 2009). The results produced by these models are only as good as the input data. A very good geological model is essential and realistic estimates of rock mass and discontinuity strengths are required.

Without reliable background information available a slope stability analysis becomes a meaningless exercise. Marinos and Hoek (2000), amongst several other experts, recommend to first describe the rock mass in geological terms before assessing it based on a point system according to the respective classification system. The advantage of this method is to gain a complete description of the rock mass independent from the classification system. The description can then be transferred to a characterization index.

There are four basic failure modes that have been observed in open pit slopes, plane failure, wedge failure, circular failure and toppling failure (fig 1). These processes of failure can occur either on their own or in different combinations and the scale of the failure can vary from a small failure on a local bench slope, to a failure of the overall pit slope. With the exception of toppling failure, all of the other failure modes involve simple gravitationally driven sliding along the planes or zones that are weaker than the remaining rock mass (Hoek, 2009). Toppling failure becomes an issue when in-dipping discontinuities create release surfaces that allow for columns of rock to topple away from the slope face.

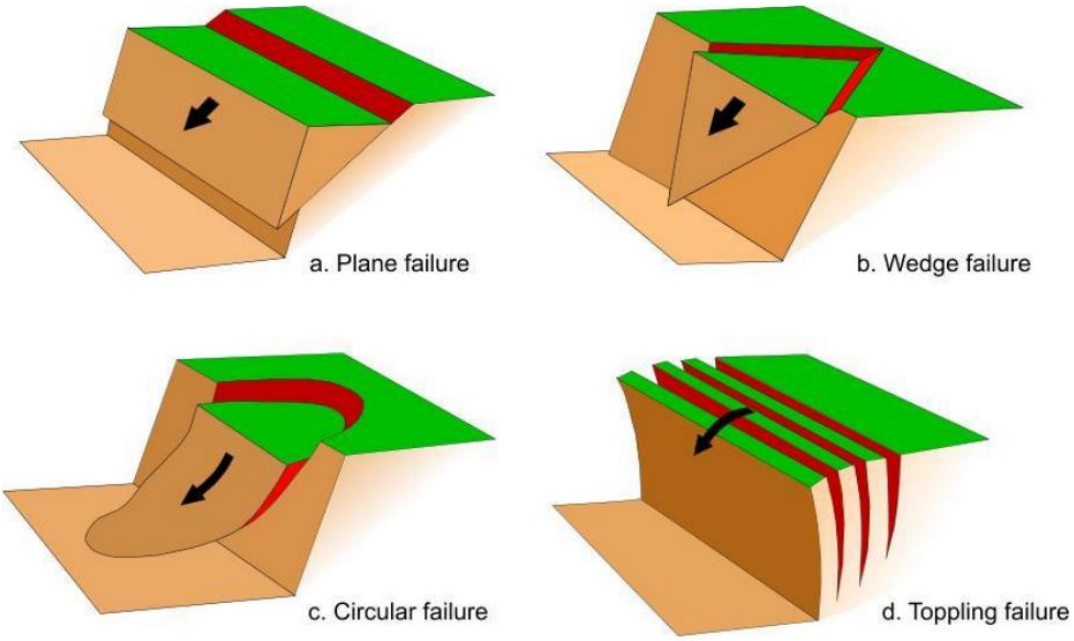

Figure 1: Illustration of most common slope failure modes. Can occur as single mode or a combination out of several modes. (Hoek, 2009)

Limit equilibrium methods for the analysis of slope stability have been available for a long time, but with the advancement in computer power in recent years have now been advanced to more effective design tools that can incorporate the most complex groundwater and geological conditions. The advantage of a limit equilibrium analysis is the simplicity and speed at which the user can examine the sensitivity of the slope by adjusting geometry, shear strength parameters, groundwater conditions and dynamic loading. Small changes in the input parameters can change the calculated result dramatically. The major disadvantage with limit equilibrium analyses in open pits is the fact that the method does not include any prediction of displacements (Hoek, 2009).

Shear Strength Reduction methods constructs a numerical model of the slope using continuum and/or discontinuum codes and once the model is constructed the shear strength of all the component materials are repeatedly increased or decreased by a Strength Reduction Factor (SRF) until the slope fails. Dawson et al. (1999) show that shear-strength reduction factors of safety are generally within a few percent of limit equilibrium analysis solutions in which the friction angle and dilation angle are equal (as cited in Hoek, 2009). The shear strength reduction method is widely used in open pit slope stability analysis since it includes all the benefits of limit equilibrium analyses, and it allows the user to study slope displacements.

1.2.1 Estimation of rock mass properties

In the case of rocks, most of the methods for estimating the shear strength of component materials for incorporation into continuum models are based on some form of rock mass classification (Hoek, 2009). Field tests to determine some of these parameters directly are time consuming, expensive and the reliability of the results of these tests is sometimes questionable (Hoek, 2005). The deformation modulus of a rock mass is an important parameter in any examination of rock mass behaviour that includes

deformations. Several authors have suggested empirical relationships for estimating the value of an isotropic rock mass deformation modulus based on classification schemes such as Rock Mass Rating (RMR), the Tunnelling Quality Index (Q) and the Geological Strength Index (GSI) (Hoek & Diederichs, 2006).

To calculate the cohesive strength *c,* it is usual to assume the friction angle ϕ. In figure 2 the relationship between the friction angle, the cohesive strength and the uniaxial compressive strength σ_{cm} of the rock mass is illustrated. According to Hoek (2009) the tensile strength of the rock mass can be estimated as about 8% of the uniaxial compressive strength $\sigma_{cm.}$ However, with the recent improvement of computer technology and numerical methods it is now possible to determine these parameters without empirical methods.

In 1971, one of the earliest papers on the modelling of discontinuous rock masses was published by Cundall, this gave rise to the development of several programs for modelling jointed rock masses and granular materials. The most recent method to analyze the behaviour of rock masses is the Synthetic Rock Mass (SRM) approach. The SRM represents a jointed rock mass and uses the Bonded Particle Model (Potyondy and Cundall, 2004) for the rock matrix and the Smooth Joint Model (Mas Ivers et al., 2008) for pre-existing fractures (as cited in Hoek, 2009). Hoek concludes that the major feature of the SRM system is that rock mass models can be built from basic properties of intact rock and rock discontinuities without having to rely on estimates based on rock mass classification systems. The joints characteristics and their orientations are obtained from drilling and mapping, then incorporated into the SRM model. Laboratory tests determine the properties of the intact rock and the discontinuities that are used in the models.

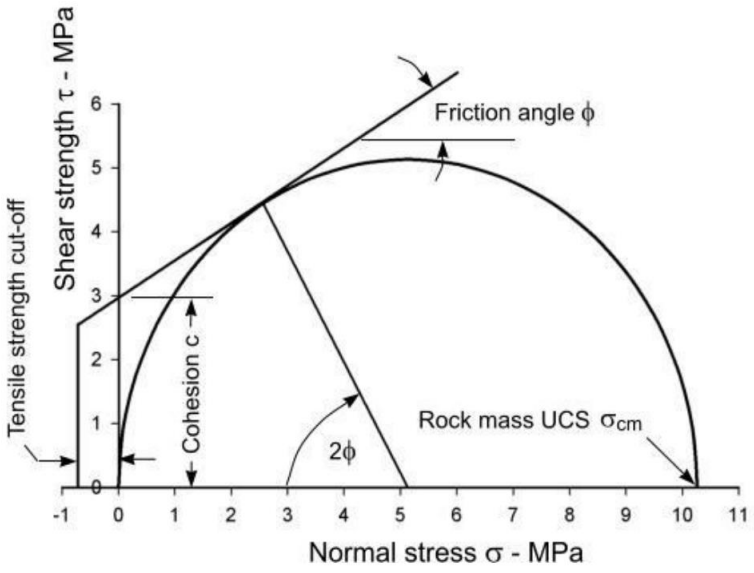

Figure 2: Mohr-Coulomb diagram showing the relationship between friction angle ϕ, cohesive strength c and uniaxial compressive strength σ_{cm} of a rock mass. The tensile strength cut-off, which is required for some slope calculations, is also presented. (Hoek, 2009).

1.2.2 Rock mass behaviour

It is argued that a rock mass behaves like cemented granular material with complex-shaped grains, both the grains and the cement are deformable and can break (Hoek, 2009). A conceptual model like this can in principle explain all aspects of mechanical behaviour.

The behaviour of rock masses is hard to determine since a rock mass includes blocks of intact rock separated by discontinuities such as joints, bedding planes, shear zones and faults. The discontinuities together with shear and tensile stresses promote rock failure. To develop a realistic model for the behaviour of such a rock mass, Potyondy and Cundall (2004, as cited in Hoek, 2009) list the following characteristics that must be considered when building a rock mass model:

- Continuously non-linear stress–strain response, with ultimate yield, followed by softening or hardening.
- Behaviour that changes in character, according to stress state; for example, crack patterns quite different in tensile, unconfined- and confined-compressive regimes.
- Memory of previous stress or strain excursions, in both magnitude and direction.
- Dilatancy that depends on history, mean stress and initial state.
- Hysteresis at all levels of cyclic loading/unloading.
- Transition from brittle to ductile shear response as the mean stress is increased.
- Dependence of incremental stiffness on mean stress and history.
- Induced anisotropy of stiffness and strength with stress and strain path.
- Non-linear envelope of strength.
- Spontaneous appearance of microcracks and localized macrofractures.
- Spontaneous emission of acoustic energy

According to Hoek (2009) most of the above characteristics can be reproduced in a SRM model but considerable work remains to be done to understand all the complex interactions that occur during the progressive failure of rock masses.

However, a long-standing problem in rock engineering is that it is impossible to conduct physical tests on samples of comparable size to the rock mass into which the slopes are excavated. While the concept of size effect has been understood for a very long time it is only with the arrival of tools such as the SRM that it has been possible to quantify this effect with any degree of certainty.

Another major feature in the SRM system is the fact that rock mass models are built from basic properties of intact rock and discontinuities without relying on estimates based on classification systems. The joint spacing, trace lengths and orientations are obtained by mapping and drilling on site, characteristics of the intact rock and discontinuities are determined from laboratory tests.

1.2.3 Wedge Sliding

The intersection of two joint planes can form a wedge which, depending on kinematic and frictional energy, could slide out. Wedges can slide on the two planes, along the line of intersection, or on one plane if that orientation is favorable over the line of intersection (Rocscience, n.d.-d).

Two planes intersecting form a line in a 3-dimensional space, the trend and plunge of the line plots as a single intersection point on a stereonet. Wedge sliding analysis is based on the analysis of intersections

and if the intersection point satisfies the kinematic and frictional conditions for sliding, it represents a risk of wedge sliding.

1.3 Rocscience software

Rocscience was formed in 1996 but the development started already in 1987 under the leadership of Dr. John Curran, at the Rock Engineering Group at the University of Toronto where they developed and distributed geomechanical software. They continue to develop geotechnical software to help professional engineers in the civil and mining industries to overcome challenges(Rocscience, n.d.-a).

1.3.1 Dips

Dips is designed for interactive analysis of orientation based geological data. Dips makes it possible to visualize orientation vectors, density contours, planes, intersections, create sets, traverses, etc. Additionally, Dips contains features to perform kinematic analyses, statistical analyses and of course stereonet plots; which will be the three main usages in this report. Dips can also investigate different ranges of slope dip, slope dip direction, friction angle and lateral limits to see how these variations influence the risk of rockfall, this is done in a kinematic sensitivity analysis.

By plotting the orientation of discontinuities in a rock mass it is possible to predict the risk of a wedge or block falling out after removal of unwanted rock is done by blasting or other procedure. Intersection points of the planes are a good guide for analyzing where potential wedges and loose blocks could fall out and are used in the kinematic analyses (Rocscience, n.d.-e). A useful rule of thumb is that any cluster with a maximum concentration of greater than 6% is very significant and a concentration less than 4% should be regarded with suspicion unless several hundreds of data points have been used(Rocscience, n.d.-b).

When performing kinematic analyses in Dips there are a few concepts that are important to understand, the first one being the friction cone (fig 3): It defines the limits of frictional stability on a stereonet. The friction angle is measured from the center of the stereonet when performing a planar sliding analysis. All poles falling outside the pole friction cone represent planes whit a steeper dip than the friction angle, and have a risk of sliding (Rocscience, n.d.-c).

Second concept is the daylight envelope (fig 3): considering pole vectors, all poles that fall within the daylight envelope represent planes which can kinematically daylight from the slope (i.e., the dip vectors of these planes point outwards from the slope)(Rocscience, n.d.-c). This, however, is only applicable for planar sliding.

A third important concept are the lateral limits (fig 3): planar failure only tends to occur when the dip direction of a plane is within a certain angular range from dip direction of the slope face. Empirical observations from Hudson and Harrison suggests an angle between 20–30° (1997, as cited by Rocscience, n.d. -b). The lateral limits add a restriction to the critical zone for planar sliding, pole vectors must be within the lateral limits in order to slide. Lateral limits are not used for wedge sliding. Since the second joint plane allows an extra degree of movement, wedges can slide over the entire lateral range.

The final concepts that will be mentioned are the primary and secondary critical zones (fig 4). The primary zone is the red crescent shaped area, intersections that plot in this zone represent wedges with a risk of sliding. In this zone wedges can slide wither on one, or two planes. The secondary critical zone are the two yellow parts of the crescent shape and here wedges can only slide on one plane. In these areas the

intersections are inclined less than the friction angle, but wedge sliding can still occur on a single joint plane which has a dip vector greater than the friction angle (Rocscience, n.d.-d).

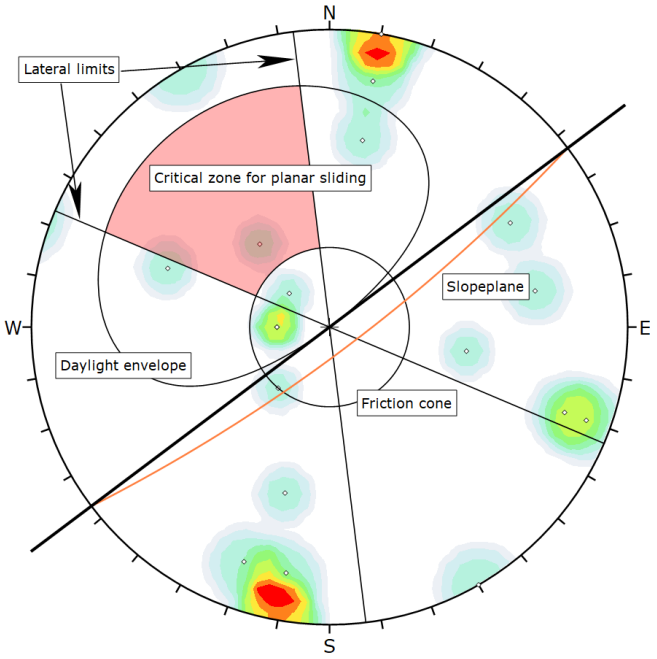

Figure 3: Explanation of the terminology used for planar sliding in Dips.

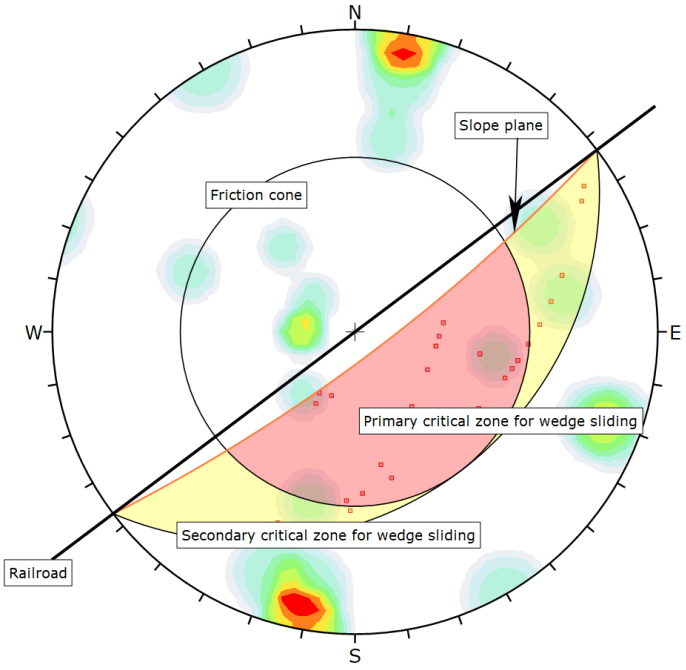

Figure 4: Explanation of the terminology used for wedge sliding in Dips.

1.3.2 SWedge

SWedge can quick and easy define tetrahedral and/or pentahedral surface wedge models formed by the intersection of two or three discontinuity planes. It can evaluate the geometry and stability of surface wedges in rock slopes using limit equilibrium methods and model the effects of shear strength, water pressure, external and seismic forces, etc. After models are created it is possible to visualize them in 3D.

The program can perform sensitivity and probabilistic analysis to determine the factor of safety and probability of failure. After a model is created it is possible to alter the geometry, joint and bedding strength, water pressure, external loads and more. A combination wedge analysis can determine the minimum factor of safety of a surface wedge by inputting any number of discrete joint plane orientations and all possible combinations of two joints forming a wedge will be analysed, this method is implemented in this work (Rocscience, n.d.-f).

2 Objective

Due to the excessive quantities of rock that fell out during the excavation of the railroad, it is of interest to see if this could have been prevented. This was done by conducting a slope stability analysis over the area of interest with the data that was available for the fractures of the rock. Models were created to determine if some wedges would have been possible to predict and avoid.

3 Study Area

The study area is located north of Gothenburg on Hisingen (fig 5). It is in the district of Eriksberg Celsiusgatan to the west and Nordviksgatan to the east. North of the area of interest is the road Säterigatan and on the southside is Östra Eriksbergsgatan.

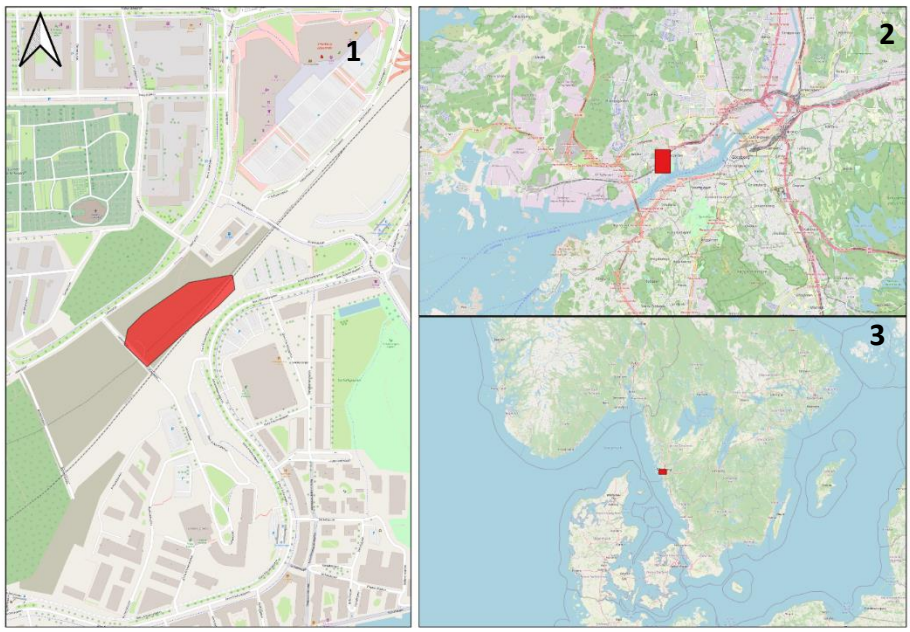

Figure 5: 1) Location of study area is shown in red. 2) An overview of the Gothenburg area, map 1 is marked with red rectangle. 3) Zoom out of southern Sweden, map 2 is marked with red rectangle.

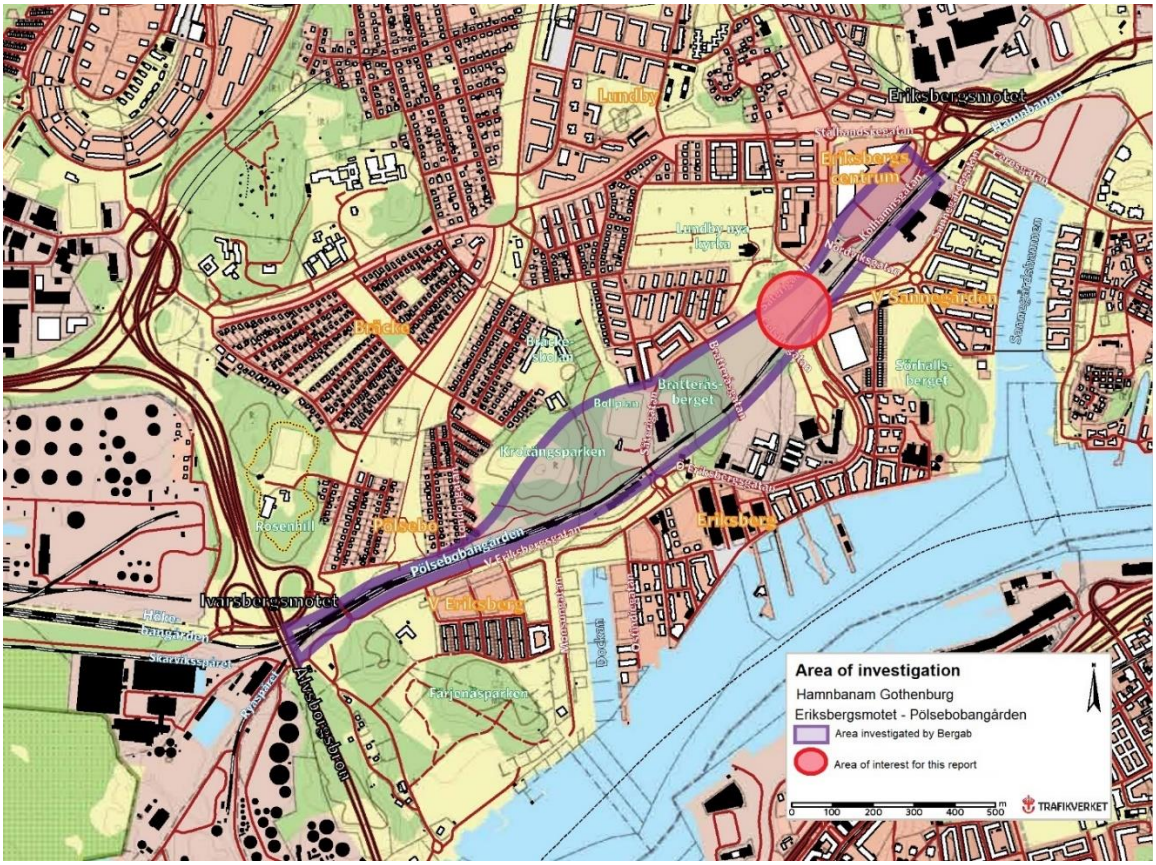

Figure 6: More detailed overview of study area including the area studied by Bergab (Karlsson, 2022).

The area where the new railroad will pass trough have been subjected to several investigations by different parties. Trafikverket have compiled much of this data into their ground technical survey, which include drill cores, soil-rock probing, mapping of the surface and of existing tunnels. Bedrock maps from the Geological Survey of Sweden (SGU) together with a rock technical investigation from Bergab (fig 6) have been used as a basis for planning the project (Trafikverket, 2018).

3.1 General geological description

According to the backing material from SGU the bedrock in the area of study is mainly granitic to granodioritic to tonalitic, weak gneissic to gneissic, often with <2 cm large potassium feldspar augen. The grain sizes vary from fine–medium to medium–coarse. The foliation is dipping steeply (65°) towards the west. The bedrock was deformed during the Sveconorwegian orogeny (1500–900 Ma) but have endured different degree of deformation, from weak to strongly gneissic. Elements of younger tectonic activity occur in the form of westerly dipping thin zones with foliation to mylonitization. Younger rock types can be observed as intrusive igneous rocks consisting of e.g., quartz and diabase.

3.2 Geological description of area of interest

The bedrock here consists mainly of a red-grey medium grain size granodiorite with 1–2cm large red phenocrysts of potassium feldspar. There is a folded gneiss that can be observed in the area with a foliation dipping towards south-west (60–85°/240°). A lighter fine-grained, equigranular granite can also be observed in the area. Minor elements of pegmatite occur.

The dominating fractures are steep–vertical with an east–westerly strike (60–90°/190°, 50–90°/010–020°) respectively northeast-southwest (60°/110°, 80–90°/290–330°). There are fractures with a weak incline towards the southeast (20–50°/110–130°) and some dipping a little steeper towards the west (50–70°/260–280°). Fracture spacing varies from 0,5 to 2 m and the fracture surfaces are normally wavy, both the smooth and the raw ones. Fracture fillings of calcite and quartz, up to 1 cm thick are prevalent and in some places coating of iron oxide occur.

4 Method

The right-hand rule was used when conducting the survey of the study area but for this paper all orientations have been converted into dip and dip direction (original data can be found in appendix A). All analyses, both in Dips and in Swedge, were performed in both a NW and SE dip direction, since the railroad will strike through the area in a NE–SW direction and rock slopes will be present on either side of the track.

4.1 Geotechnical investigation

Mapping of the outcrops in the area was done by Bergarb according to Geotechnical Field manual (Geoteknisk Fälthandbok, SGF 1:96). The mapping was performed in March 2013 to March 2014 over an area of 92 000m^2 where visible rock was available, locations with soil depth less than 0,5 m was excavated to expose rock. Rock type, colour, structures and fracture properties were recorded. Measurements of the structures strike and dip was done according to the right-hand rule (Trafikverket, 2018). A total of 91 measurements were recorded above ground, 19 of these were taken in the area of interest for this project. Two scan line surveys of 20 m each was performed below surface in an already existing tunnel, this resulted in 62 data points used for estimation of fracture sets.

4.2 Collection of additional orientational data

To evaluate the original orientational measurements taken by Bergab, the section of interest was examined by the author of this report after the slope was constructed. Orientational data was collected with the use of a clar-compass which have a bull's eye spirit level attached. This level enables the possibility of acquiring the true dip and dip direction easier. However, these measurements where not used in the analyses but merely to appraise the original data obtained. This was done by creating four different plots, two with the datapoints from Bergab and two plots with orientational data collected by myself. The data points were divided into sets and a mean value for the sets were recorded. The dataset that was collected by the author was divided into two different ways to see how this affects the result.

When orientations were measured it was clear that the discontinuities are not completely straight and that they could differ several degrees in less than half a meter. The compass has a small surface area, so to be able to interpolate, a hardcover book was used as underlay to get an average of the discontinuity's orientation.

4.3 Analysis of orientation data in Dips

Using the acquired data in the software Dips from Rocscience, it is possible to get a good overview of how structures in the area are oriented, how they intersect and where potential slides, rockfalls or wedges could occur.

An excel file with all the relevant data obtained from Bergabs fieldwork was created that later could be imported into Dips via the Import Wizard. It is beneficial to make sure that the global orientation format

in the project settings for the Dips-file match the method that was used when the data was collected, in this case the right-hand rule. The data can then easily be converted into desired orientation format, for this study Dip/Dip Direction have been used. A black line was added to symbolize the railroad in the N-E/S-W direction (Strike of 143°) and two kinematic analyses were performed in Dips: planar sliding and wedge sliding.

To perform a planar sliding analysis in Dips, simply enter the dip and dip direction of the desired finished plane orientation together with a friction angle and lateral limits, then the program will do the rest to calculate potential sliding planes. Adjacent poles were grouped together in sets, which made it possible to examine the mean values of structures with similar orientation. The number of poles within the critical zone are counted, results are expressed as a percentage of all poles in the file, and as a percentage of poles within individual sets (if sets are defined).

Kinematic wedge sliding analysis was performed with the same inputs of desired slope result together with the friction angle. However, it is important to include the intersection points of all structures for the program to compute where wedges potentially could fall out. The number of intersections within the critical zone is counted, results are expressed as a percentage of all intersections. This percentage gives an estimate of "probability of failure" with respect to the total number of intersections.

A slope dip of 80° were used for the initial analyse together with a friction angle of 30° and lateral limits of 30°. Analyses were performed on two different data sets, one with 19 data points from the direct vicinity of the area of interest and another one with all the 91 data points recorded for the area.

Sensitivity analyses were conducted within a certain range of the parameters. The slope dip was set from 50 to 90° and the dip direction was analyzed 35° on either side from the desired railroad strike of 143/323°. The range of the friction angle was tested from 15–50° and lateral limits was also set to 15-50°.

4.4 Wedge Sliding in SWedge

To determine the minimum factor of safety for a surface wedge, SWedge from Rocscience was used. In the project settings the analysis type was set to combination wedge analysis which allows the user to enter any number of joint plane orientations and all possible combinations of two joints forming a wedge will be analyzed. When analysing the kinematic wedge sliding the density contours are switched to intersection mode to show density of intersections instead of pole vectors. When the maximum contour concentrations overlap the critical zone, wedge sliding is most likely going to be a problem. The units and block shape were set to metric and wedge shape respectively. Sampling method was set to Latin Hypercube with 10000 number of samples and the random number generation was set to pseudo-random (each time the analysis is run, exactly the same results will be given for a certain seed value)

The combinations input data for the slope was set to a dip degree of 70/80/90° and dip direction of 143/323°. The height of the slope is 15m, it is roughly 30m long and bench width was set to 10m. A standard value of 0,026MN/m^3 for the density of granite was used for unit weight in the rock properties section and the minimum wedge size was determined to be at 0,001MN (≈102kg). The slope length is in the same direction as the strike of the slope, defining the slope length is another method of limiting the size of the wedges. Bench width is the extent of the upper face measured perpendicular to the slope crest. This distance is measured in the horizontal plane. Wedges that exceed these limits are scaled down so that they fit the slope dimensions.

5 Results

After analysing the fracture data from the mapping, conducted by Bergab, a friction angle of 30° was used for the fracture planes. Furthermore, it is clear from figure 18 and 19 that unless very low values for friction angle is used it does not affect the critical percentage for wedge sliding in any major way.

5.1 Comparison of data sets

The data provided by Bergab (fig 7a&b) was compared with data collected by the author (fig 7c&d) and divided into different discontinuity sets. A summary of the dip and dip directions of the mean planes can be seen in table 1.

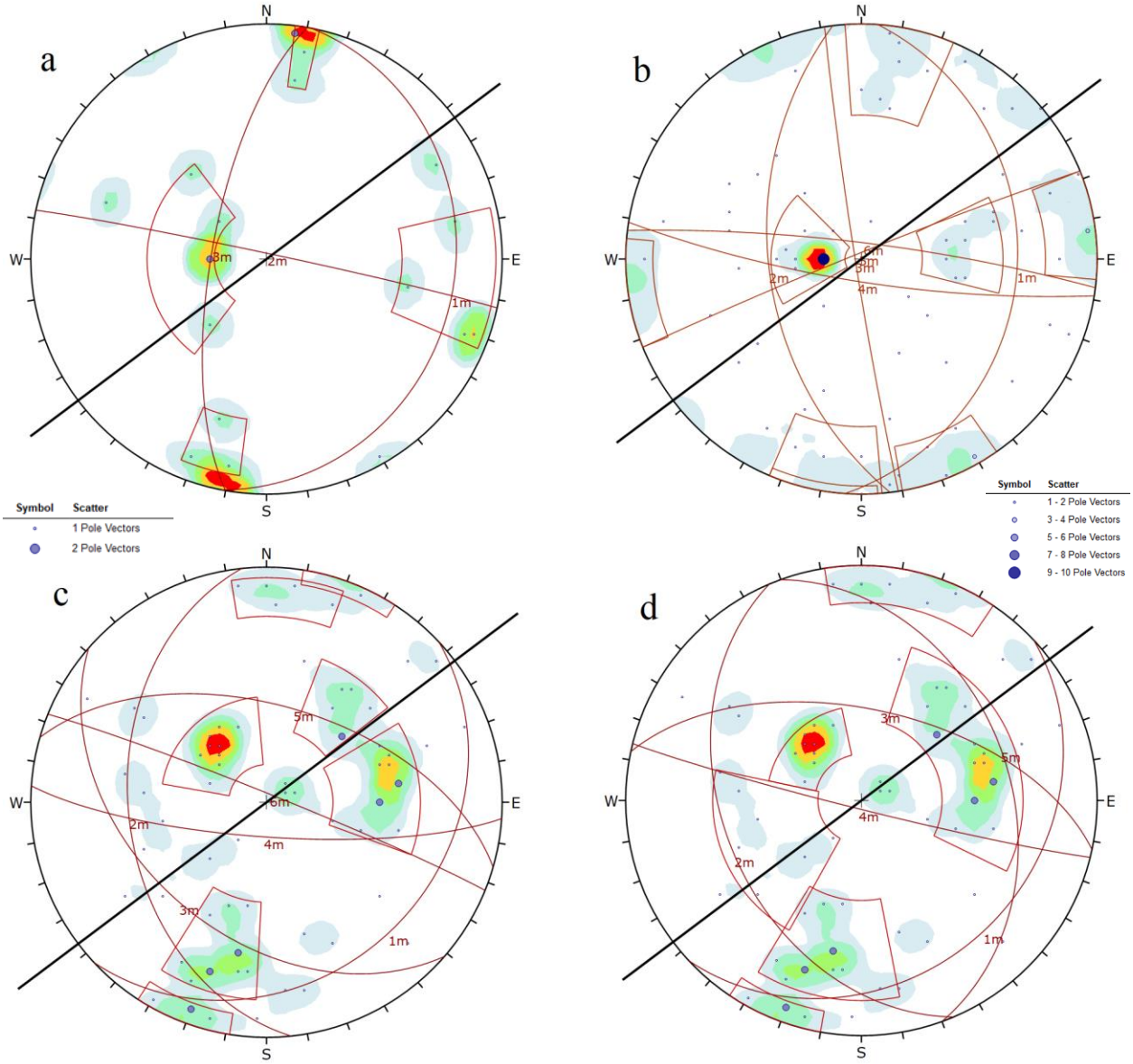

Figure 7: Stereonets from the different datasets. Mean values from the planes are shown in red great circles and the railroad is symbolized by the thick black line striking in NE-SW direction. The curvilinear, four-sided windows are the respective sets for each great circle.
a) 19 datapoints b) 91 data points. c) 74 datapoints with six sets. d) 74 datapoints with five sets.

Table 1: Mean values of dip and dip direction from the different data sets.

19 datapoints Figure 7a			**91 datapoints** Figure 7b			**74 datapoints** Figure 7c			**74 datapoints** Figure 7d		
ID	**Dip**	**Dip Direction**	**ID**	**Dip**	**Dip Direction**	**ID**	**Dip**	**Dip Direction**	**ID**	**Dip**	**Dip Direction**
1m	21,04	101,08	1m	23,35	94,15	1m	25,33	136,84	1m	25,33	136,84
2m	87,86	12,1	2m	46,99	262,94	2m	40,78	263,94	2m	40,77	247,28
3m	70,91	280,36	3m	87,48	261,02	3m	42,6	220,96	3m	58,16	11,91
			4m	78,71	189,45	4m	78,48	184,16	4m	87,17	194,4
			5m	87,2	337,77	5m	56,29	16,13	5m	36,54	70,26
			6m	82,42	7,46	6m	87,18	22			

5.2 Dips

Analyses in Dips result in a relatively high risk that wedge sliding will occur, especially when taking the shear zones in consideration. In the sensitivity analysis the slope dip, together with friction angle and lateral limits, shows as the biggest contributors towards slope failure. There is no indication that planar failure will occur.

5.2.1 Kinematic analyses

The first kinematic analyses in Dips revealed that planar sliding should not be a problem in either case, but wedge sliding can become a problem.

5.2.1.1 Planar Sliding

The kinematic analyses performed for planar sliding in Dips show no indication that a plane failure will occur in either direction. The first investigation showed a 5,26% risk that planar sliding will happen on the north-western slope (fig 8) and a zero percent risk for sliding to occur on the south-west slope (fig 9). The second analysis were performed with 91 data points (instead of 19) and display a similar result with only a 5,49% risk that sliding will occur in either direction (fig 10&11).

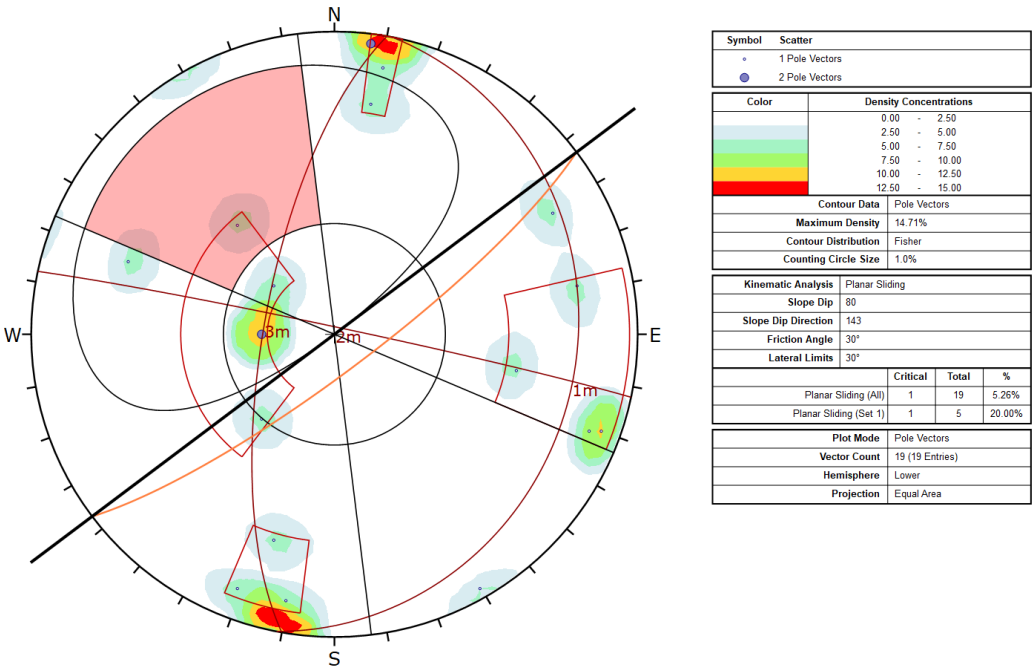

Symbol	Scatter
	1 Pole Vectors
	2 Pole Vectors

Color	Density Concentrations
	0.00 - 2.50
	2.50 - 5.00
	5.00 - 7.50
	7.50 - 10.00
	10.00 - 12.50
	12.50 - 15.00

Contour Data	Pole Vectors
Maximum Density	14.71%
Contour Distribution	Fisher
Counting Circle Size	1.0%

Kinematic Analysis	Planar Sliding
Slope Dip	80
Slope Dip Direction	143
Friction Angle	30°
Lateral Limits	30°

	Critical	Total	%
Planar Sliding (All)	1	19	5.26%
Planar Sliding (Set 1)	1	5	20.00%

Plot Mode	Pole Vectors
Vector Count	19 (19 Entries)
Hemisphere	Lower
Projection	Equal Area

Figure 8: Planar sliding analysis executed on north-western slope with a dip/dip direction of 80°/143° and a vector count of 19.

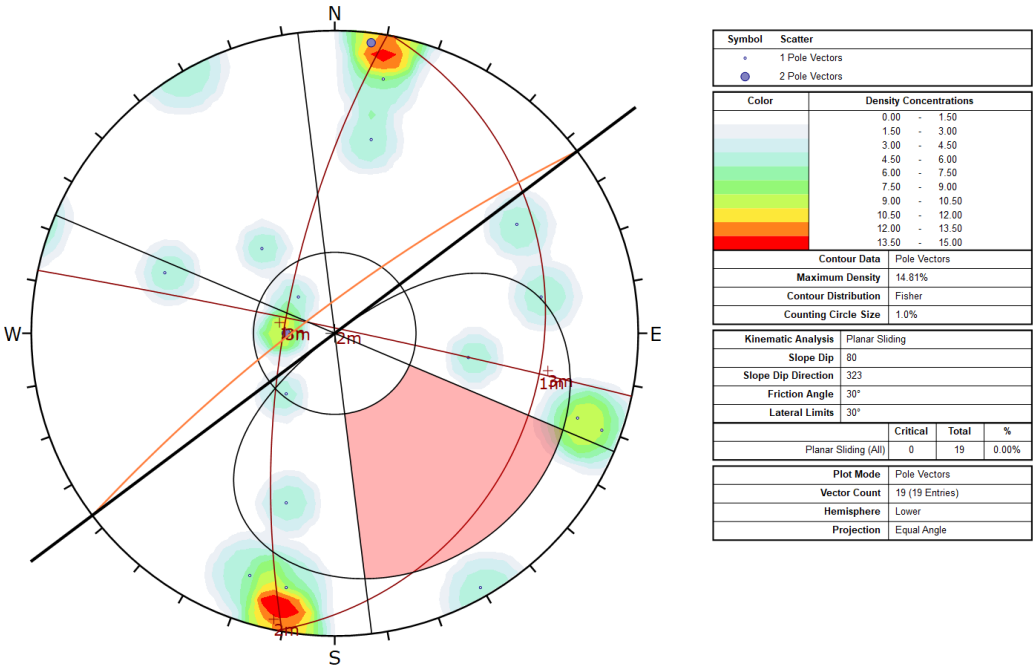

Symbol	Scatter
	1 Pole Vectors
	2 Pole Vectors

Color	Density Concentrations
	0.00 - 1.50
	1.50 - 3.00
	3.00 - 4.50
	4.50 - 6.00
	6.00 - 7.50
	7.50 - 9.00
	9.00 - 10.50
	10.50 - 12.00
	12.00 - 13.50
	13.50 - 15.00

Contour Data	Pole Vectors
Maximum Density	14.81%
Contour Distribution	Fisher
Counting Circle Size	1.0%

Kinematic Analysis	Planar Sliding
Slope Dip	80
Slope Dip Direction	323
Friction Angle	30°
Lateral Limits	30°

	Critical	Total	%
Planar Sliding (All)	0	19	0.00%

Plot Mode	Pole Vectors
Vector Count	19 (19 Entries)
Hemisphere	Lower
Projection	Equal Angle

Figure 9: Planar sliding analysis executed on south-eastern slope with a dip/dip direction of 80°/323° and a vector count of 19.

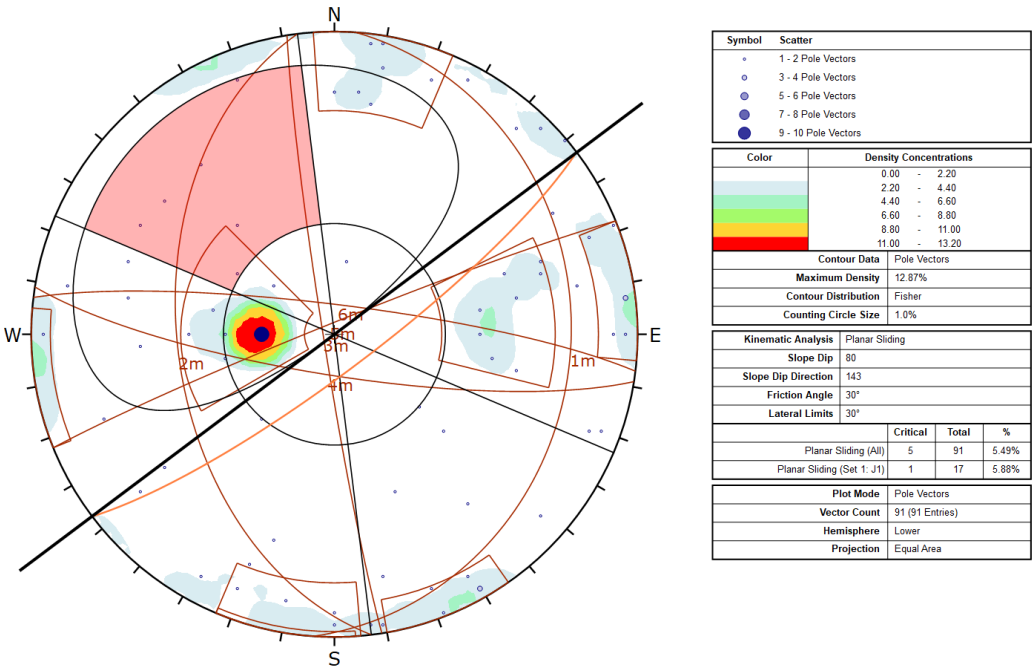

Symbol	Scatter
	1 - 2 Pole Vectors
	3 - 4 Pole Vectors
	5 - 6 Pole Vectors
	7 - 8 Pole Vectors
	9 - 10 Pole Vectors

Color	Density Concentrations
	0.00 - 2.20
	2.20 - 4.40
	4.40 - 6.60
	6.60 - 8.80
	8.80 - 11.00
	11.00 - 13.20

Contour Data	Pole Vectors
Maximum Density	12.87%
Contour Distribution	Fisher
Counting Circle Size	1.0%

Kinematic Analysis	Planar Sliding
Slope Dip	80
Slope Dip Direction	143
Friction Angle	30°
Lateral Limits	30°

	Critical	Total	%
Planar Sliding (All)	5	91	5.49%
Planar Sliding (Set 1: J1)	1	17	5.88%

Plot Mode	Pole Vectors
Vector Count	91 (91 Entries)
Hemisphere	Lower
Projection	Equal Area

Figure 10: Planar sliding analysis executed on north-western slope with a dip/dip direction of 80°/143° and a vector count of 91.

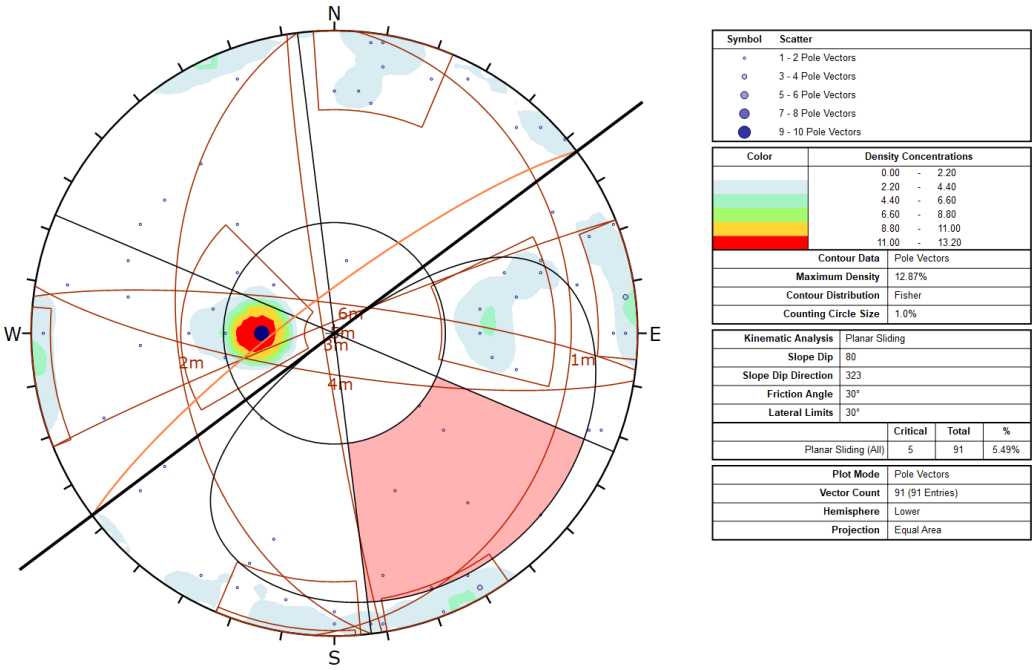

Symbol	Scatter
	1 - 2 Pole Vectors
	3 - 4 Pole Vectors
	5 - 6 Pole Vectors
	7 - 8 Pole Vectors
	9 - 10 Pole Vectors

Color	Density Concentrations
	0.00 - 2.20
	2.20 - 4.40
	4.40 - 6.60
	6.60 - 8.80
	8.80 - 11.00
	11.00 - 13.20

Contour Data	Pole Vectors
Maximum Density	12.87%
Contour Distribution	Fisher
Counting Circle Size	1.0%

Kinematic Analysis	Planar Sliding
Slope Dip	80
Slope Dip Direction	323
Friction Angle	30°
Lateral Limits	30°

	Critical	Total	%
Planar Sliding (All)	5	91	5.49%

Plot Mode	Pole Vectors
Vector Count	91 (91 Entries)
Hemisphere	Lower
Projection	Equal Area

Figure 11: Planar sliding analysis executed on south-eastern slope with a dip/dip direction of 80°/323° and a vector count of 91.

5.2.1.2 Wedge Sliding

Kinematic wedge sliding analyses with 19 datapoints show that there is already quite a significant risk of wedge sliding in both directions, it is slightly higher on the north-western slope (fig 12) with a 18,34% risk of wedges sliding compared to 13,61% on the southeast slope (fig 13).

When adding the rest of the dataset to reach the total of 91 vector counts the results changes slightly. The north-western slope's (fig 14) risk of wedge sliding decreases to 18,08% whereas the southeast slope (fig 15) increases to 20,69%.

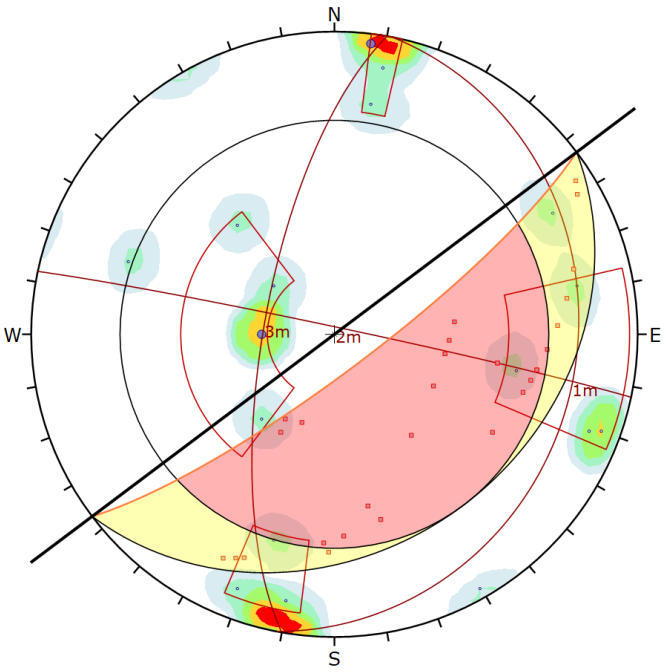

Symbol	Scatter
	1 Pole Vectors
	2 Pole Vectors
Symbol	**Feature**
	Critical Intersection

Color	Density Concentrations
	0.00 - 2.50
	2.50 - 5.00
	5.00 - 7.50
	7.50 - 10.00
	10.00 - 12.50
	12.50 - 15.00

Contour Data	Pole Vectors
Maximum Density	14.71%
Contour Distribution	Fisher
Counting Circle Size	1.0%

Kinematic Analysis	Wedge Sliding
Slope Dip	80
Slope Dip Direction	143
Friction Angle	30°

	Critical	Total	%
Wedge Sliding	31	169	18.34%

Plot Mode	Pole Vectors
Vector Count	19 (19 Entries)
Intersection Mode	Grid Data Planes
Intersections Count	169
Hemisphere	Lower
Projection	Equal Area

Figure 12: Kinematic wedge sliding analysis performed on north-western slope with a dip/dip direction of 80°/143° and a vector count of 19.

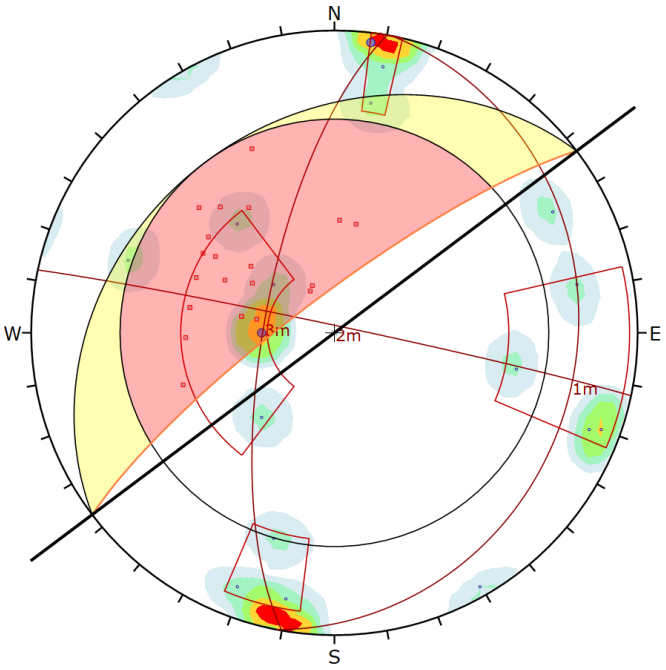

Symbol	Scatter
	1 Pole Vectors
	2 Pole Vectors
Symbol	**Feature**
	Critical Intersection

Color	Density Concentrations
	0.00 - 2.50
	2.50 - 5.00
	5.00 - 7.50
	7.50 - 10.00
	10.00 - 12.50
	12.50 - 15.00

Contour Data	Pole Vectors
Maximum Density	14.71%
Contour Distribution	Fisher
Counting Circle Size	1.0%

Kinematic Analysis	Wedge Sliding
Slope Dip	80
Slope Dip Direction	323
Friction Angle	30°

	Critical	Total	%
Wedge Sliding	23	169	13.61%

Plot Mode	Pole Vectors
Vector Count	19 (19 Entries)
Intersection Mode	Grid Data Planes
Intersections Count	169
Hemisphere	Lower
Projection	Equal Area

Figure 13: Wedge sliding analysis performed on south-eastern slope with a dip/dip direction of 80°/323° and a vector count of 19.

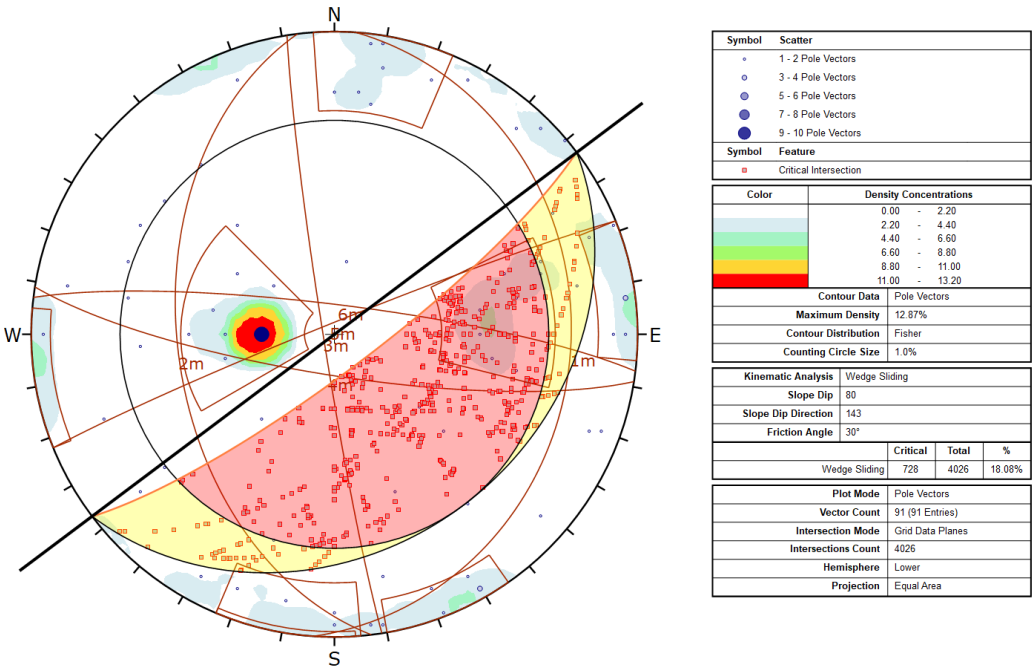

Symbol	Scatter
	1 - 2 Pole Vectors
	3 - 4 Pole Vectors
	5 - 6 Pole Vectors
	7 - 8 Pole Vectors
	9 - 10 Pole Vectors
Symbol	**Feature**
	Critical Intersection

Color	Density Concentrations
	0.00 - 2.20
	2.20 - 4.40
	4.40 - 6.60
	6.60 - 8.80
	8.80 - 11.00
	11.00 - 13.20

Contour Data	Pole Vectors
Maximum Density	12.87%
Contour Distribution	Fisher
Counting Circle Size	1.0%

Kinematic Analysis	Wedge Sliding
Slope Dip	80
Slope Dip Direction	143
Friction Angle	30°

	Critical	Total	%
Wedge Sliding	728	4026	18.08%

Plot Mode	Pole Vectors
Vector Count	91 (91 Entries)
Intersection Mode	Grid Data Planes
Intersections Count	4026
Hemisphere	Lower
Projection	Equal Area

Figure 14: Wedge sliding analysis performed on north-western slope with a dip/dip direction of 80°/143° and a vector count of 91.

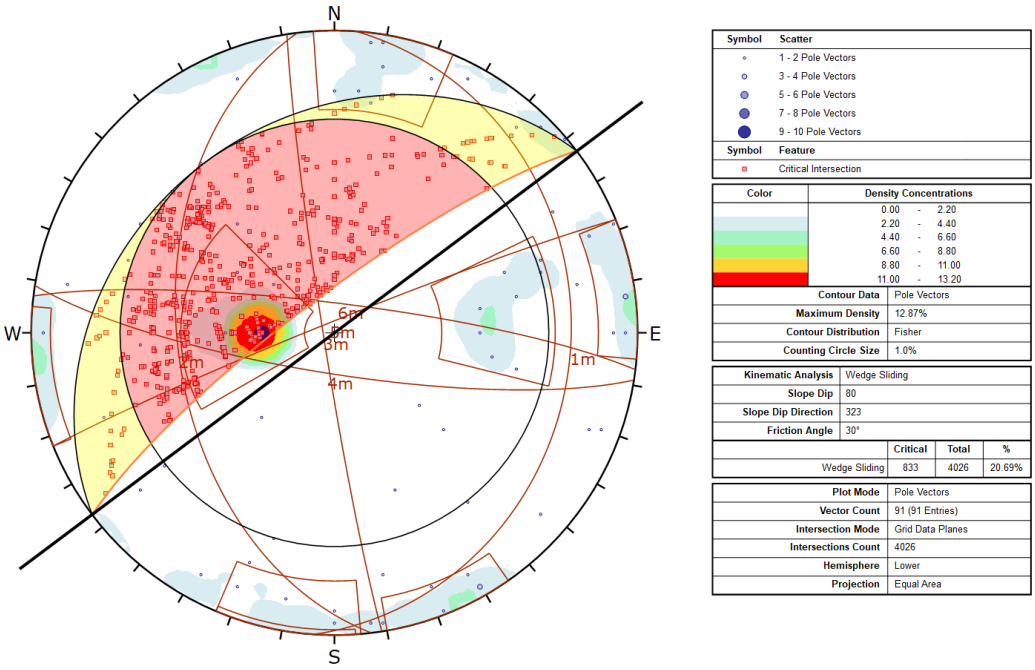

Symbol	Scatter
	1 - 2 Pole Vectors
	3 - 4 Pole Vectors
	5 - 6 Pole Vectors
	7 - 8 Pole Vectors
	9 - 10 Pole Vectors
Symbol	**Feature**
	Critical Intersection

Color	Density Concentrations
	0.00 - 2.20
	2.20 - 4.40
	4.40 - 6.60
	6.60 - 8.80
	8.80 - 11.00
	11.00 - 13.20

Contour Data	Pole Vectors
Maximum Density	12.87%
Contour Distribution	Fisher
Counting Circle Size	1.0%

Kinematic Analysis	Wedge Sliding
Slope Dip	80
Slope Dip Direction	323
Friction Angle	30°

	Critical	Total	%
Wedge Sliding	833	4026	20.69%

Plot Mode	Pole Vectors
Vector Count	91 (91 Entries)
Intersection Mode	Grid Data Planes
Intersections Count	4026
Hemisphere	Lower
Projection	Equal Area

Figure 15: Wedge sliding analysis performed on south-eastern slope with a dip/dip direction of 80°/323° and a vector count of 91.

When examining different types of discontinuities in the area, particularly the shear zones, they intersect with the mean set planes within the zone for critical wedge sliding on the south-eastern side of the railroad hence the risk for wedge sliding is increased to 32,14% (fig 16). Furthermore, if the slope dip is increased to 90° the risk for wedge sliding increases to 46,43%, additionally the intersection contour falls within the primary critical zone for wedge sliding (fig 17).

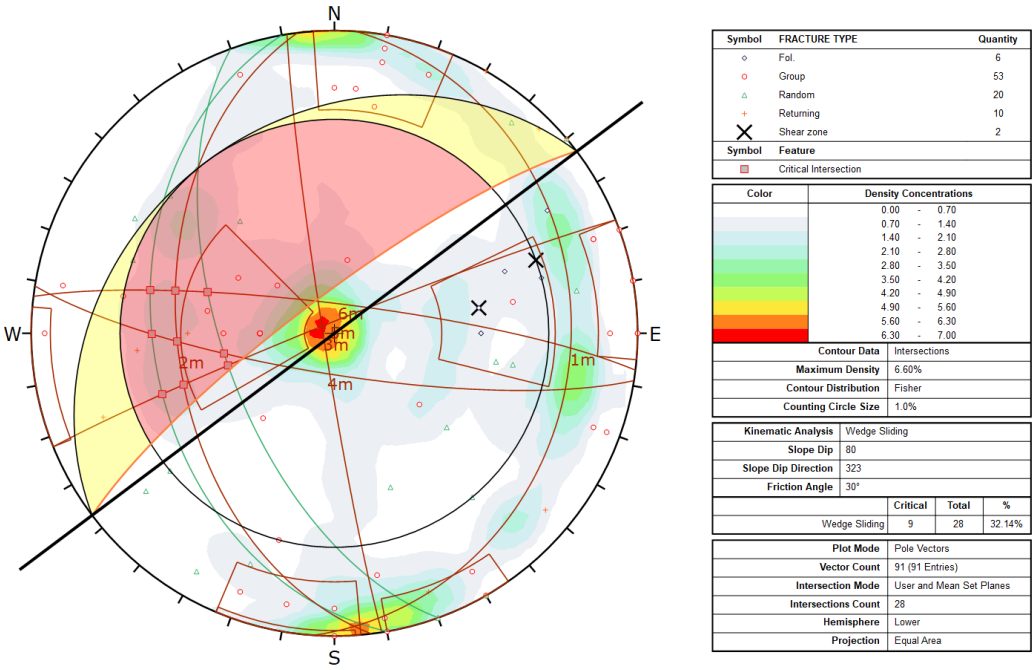

Symbol	FRACTURE TYPE	Quantity
◇	Fol.	6
○	Group	53
△	Random	20
+	Returning	10
X	Shear zone	2

Symbol	Feature
▢	Critical Intersection

Color	Density Concentrations
	0.00 - 0.70
	0.70 - 1.40
	1.40 - 2.10
	2.10 - 2.80
	2.80 - 3.50
	3.50 - 4.20
	4.20 - 4.90
	4.90 - 5.60
	5.60 - 6.30
	6.30 - 7.00

Contour Data	Intersections
Maximum Density	6.60%
Contour Distribution	Fisher
Counting Circle Size	1.0%

Kinematic Analysis	Wedge Sliding
Slope Dip	80
Slope Dip Direction	323
Friction Angle	30°

	Critical	Total	%
Wedge Sliding	9	28	32.14%

Plot Mode	Pole Vectors
Vector Count	91 (91 Entries)
Intersection Mode	User and Mean Set Planes
Intersections Count	28
Hemisphere	Lower
Projection	Equal Area

Figure 16: Kinematic wedge analysis performed on south-eastern slope with dip/dip direction of 80°/323° with the shear zones showing with green lines.

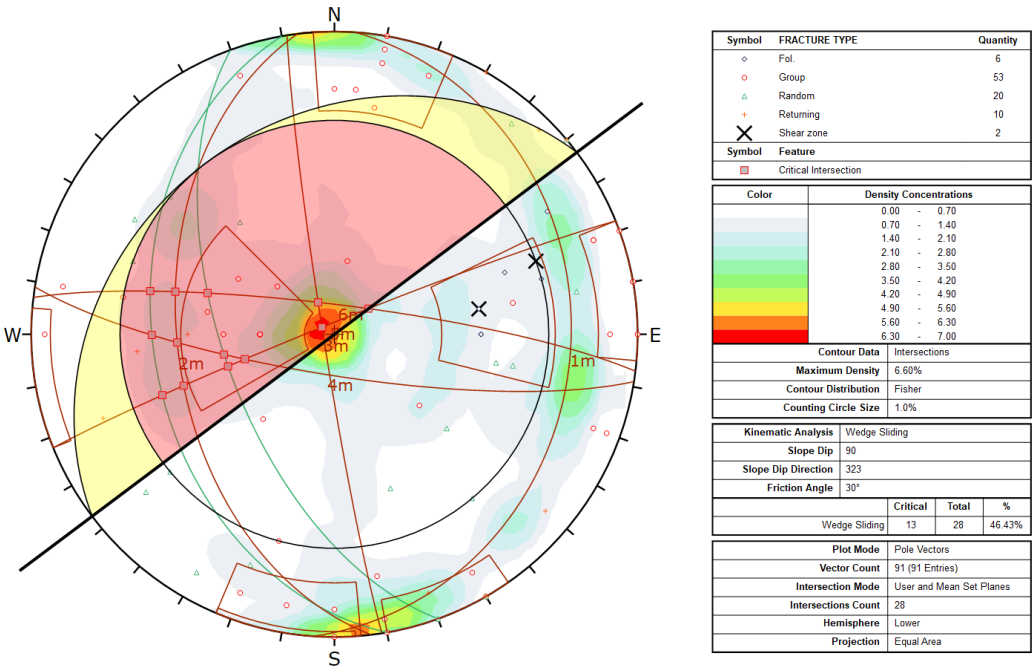

Symbol	FRACTURE TYPE	Quantity
◇	Fol.	6
○	Group	53
△	Random	20
+	Returning	10
X	Shear zone	2

Symbol	Feature
▭	Critical Intersection

Color	Density Concentrations
	0.00 - 0.70
	0.70 - 1.40
	1.40 - 2.10
	2.10 - 2.80
	2.80 - 3.50
	3.50 - 4.20
	4.20 - 4.90
	4.90 - 5.60
	5.60 - 6.30
	6.30 - 7.00

Contour Data	Intersections
Maximum Density	6.60%
Contour Distribution	Fisher
Counting Circle Size	1.0%

Kinematic Analysis	Wedge Sliding
Slope Dip	90
Slope Dip Direction	323
Friction Angle	30°

	Critical	Total	%
Wedge Sliding	13	28	46.43%

Plot Mode	Pole Vectors
Vector Count	91 (91 Entries)
Intersection Mode	User and Mean Set Planes
Intersections Count	28
Hemisphere	Lower
Projection	Equal Area

Figure 17: South-eastern slope with dip/dip direction of 90°/323° and a risk of 46,43% risk of sliding when only set mean planes and shear zones are considered.

5.2.2 Kinematic Sensitivity

Kinematic sensitivity analyses indicated that a steeper slope dip angle is the biggest contributor to failing rocks in this case.

5.2.2.1 Planar sliding

The risk for planar sliding was not affected particularly, depending on if the sensitivity analysis was performed with 19 or 91 vector points. When executed with 19 points only the slope dip direction and the lateral limits were affecting the risk for planar sliding as can be seen in figure 18. When complementing with the rest of the data points it is obvious that a steeper dip degree become a bigger issue when the dip angle is >80° but not until reaching above 89° it crosses a critical percentage of more than 10 % planar sliding (fig 19).

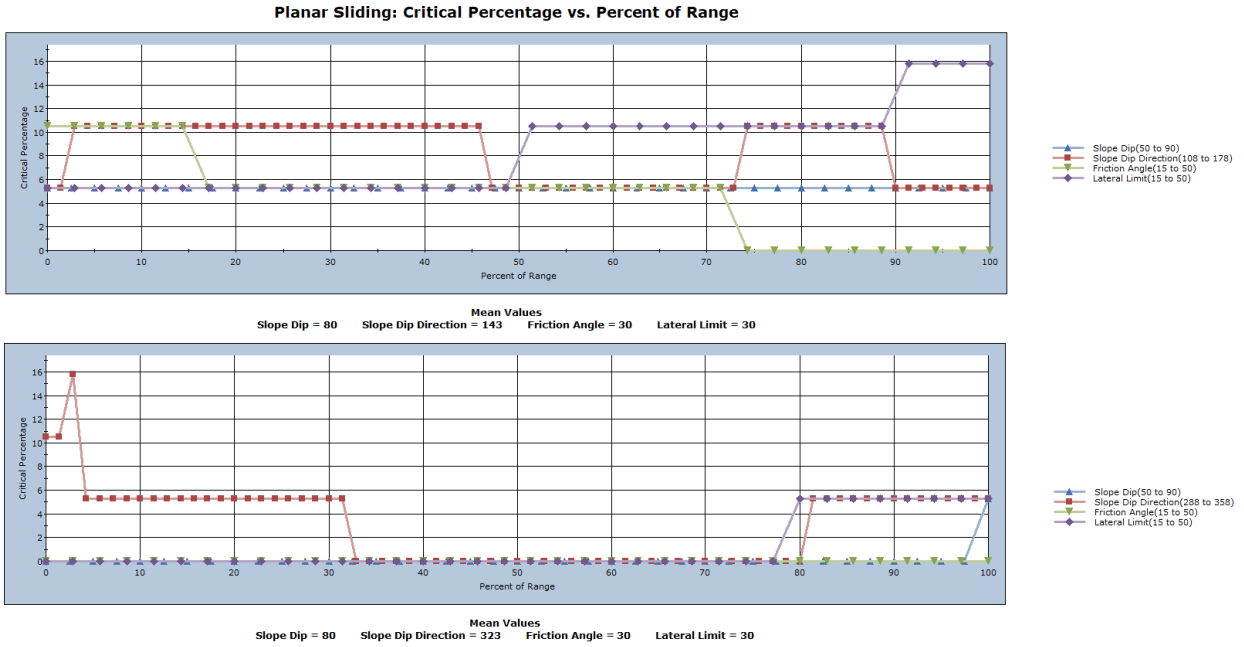

Figure 18: Kinematic sensitivity analysis for planar sliding conducted with 19 data points. In the upper figure the analysis is performed on the north-western slope and in the lower the analysis is performed on the southeast slope.

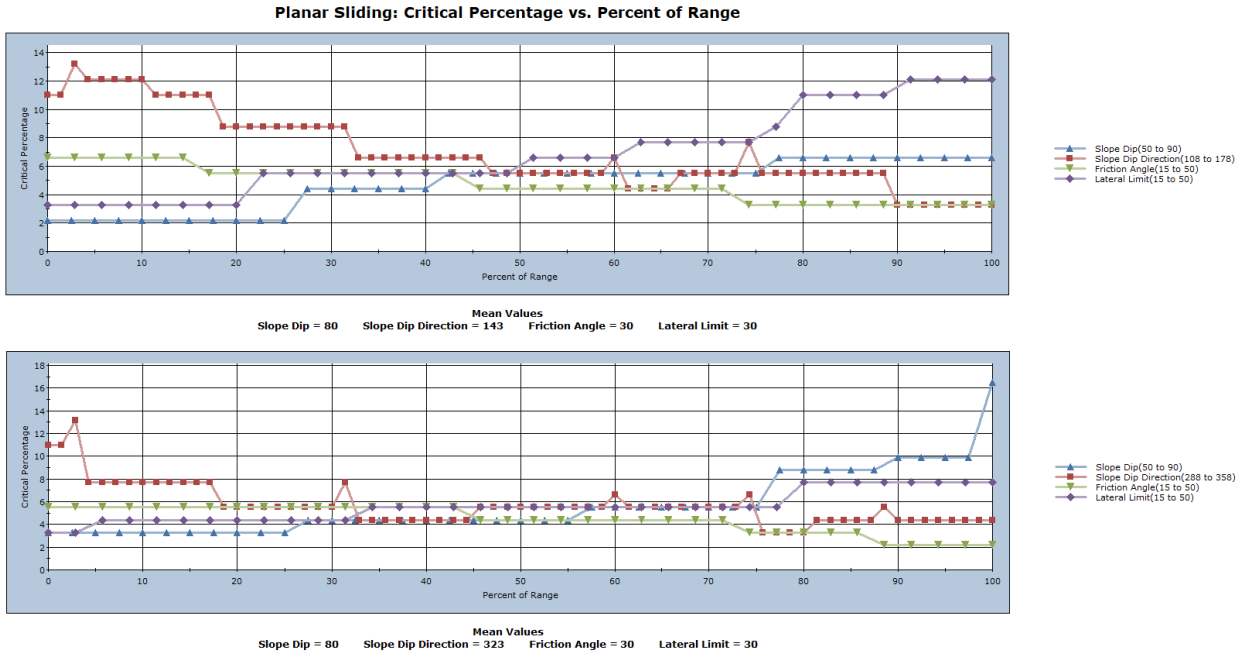

Figure 19: Kinematic sensitivity analysis for planar sliding conducted with 91 data points. In the upper figure the analysis is performed on the north-western slope and in the lower the analysis is performed on the southeast slope.

5.2.2.2 *Wedge sliding*

When analysing the sensitivity of kinematic wedge sliding the diagrams show a great increase in critical percentage of failing wedges with an increase of the slope dip. Very low values of friction angle also yield high percentage of failing wedges whereas the slope dip direction does not seem to influence in any major way, this is the case for all four scenarios (figure 20&21, either direction with 19 or 91 data points).

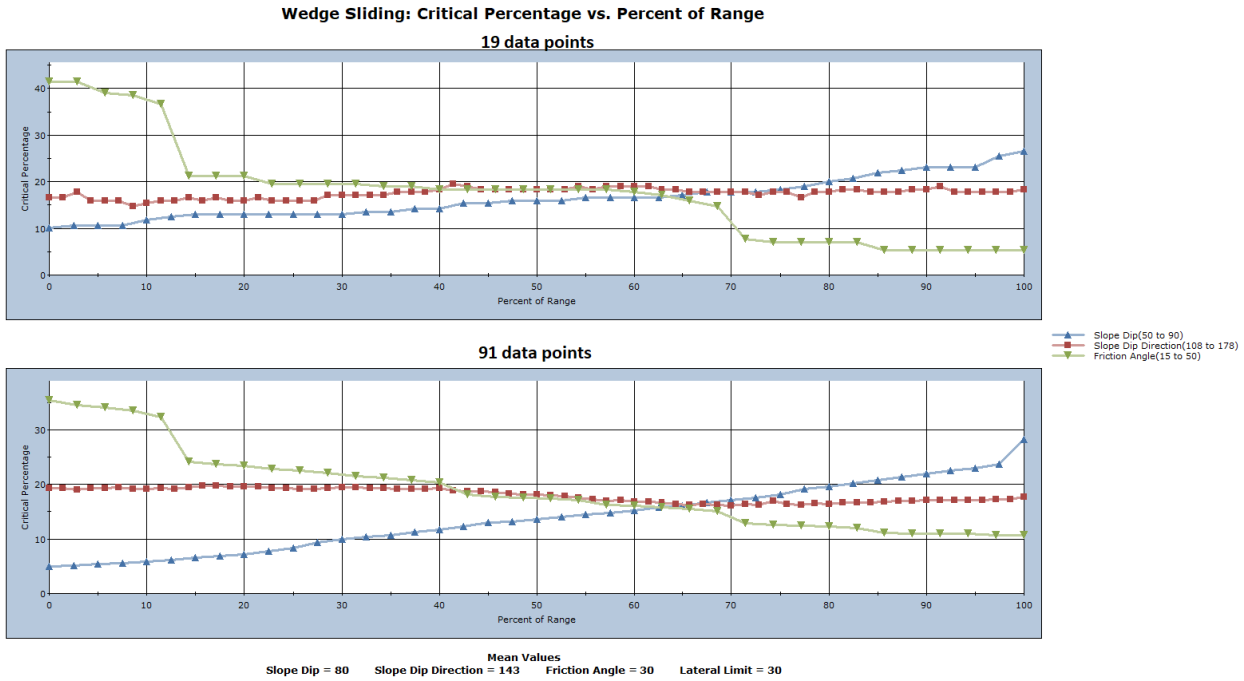

Figure 20: Kinematic sensitivity analysis of wedge sliding on the north-western slope.

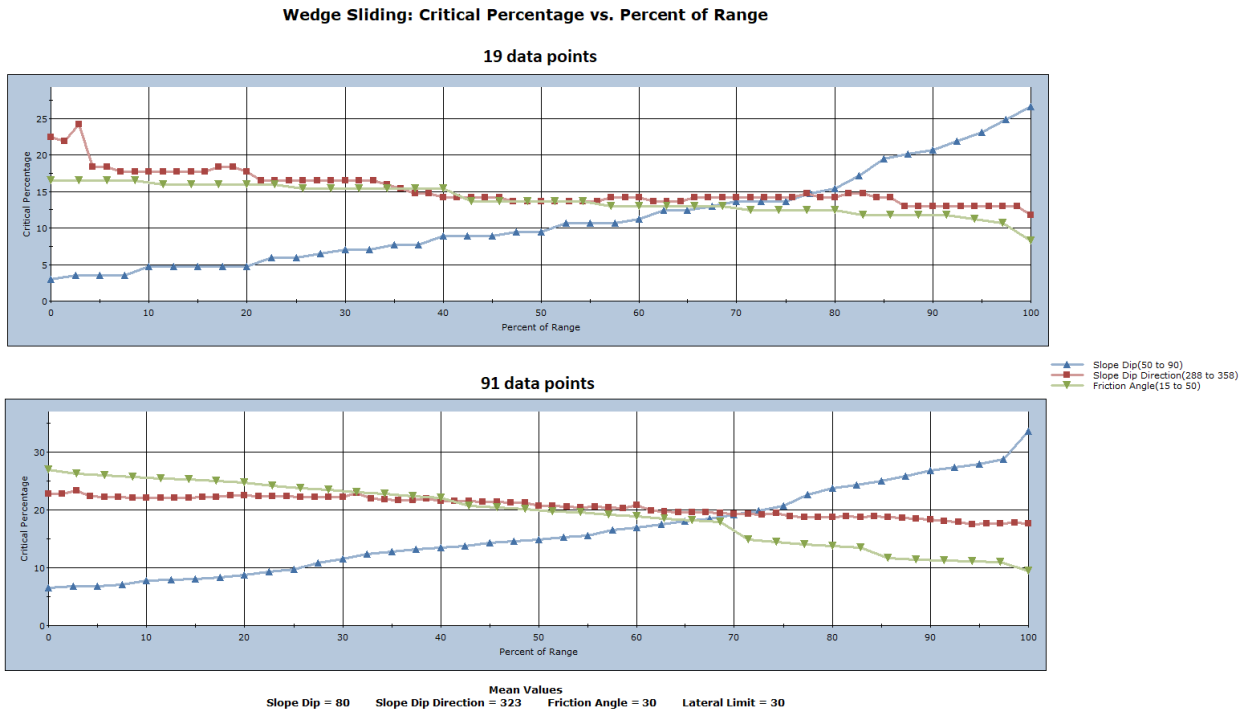

Figure 21: Kinematic sensitivity analysis of wedge sliding on the south-eastern slope.

5.3 SWedge

The north-western slope's most unstable wedge has a factor of safety of 0,50 from 164 failed wedges and 1508 valid wedges, this result in a probability of failure of 10,9%, this is when a slope dip of 70° is considered (fig 22).

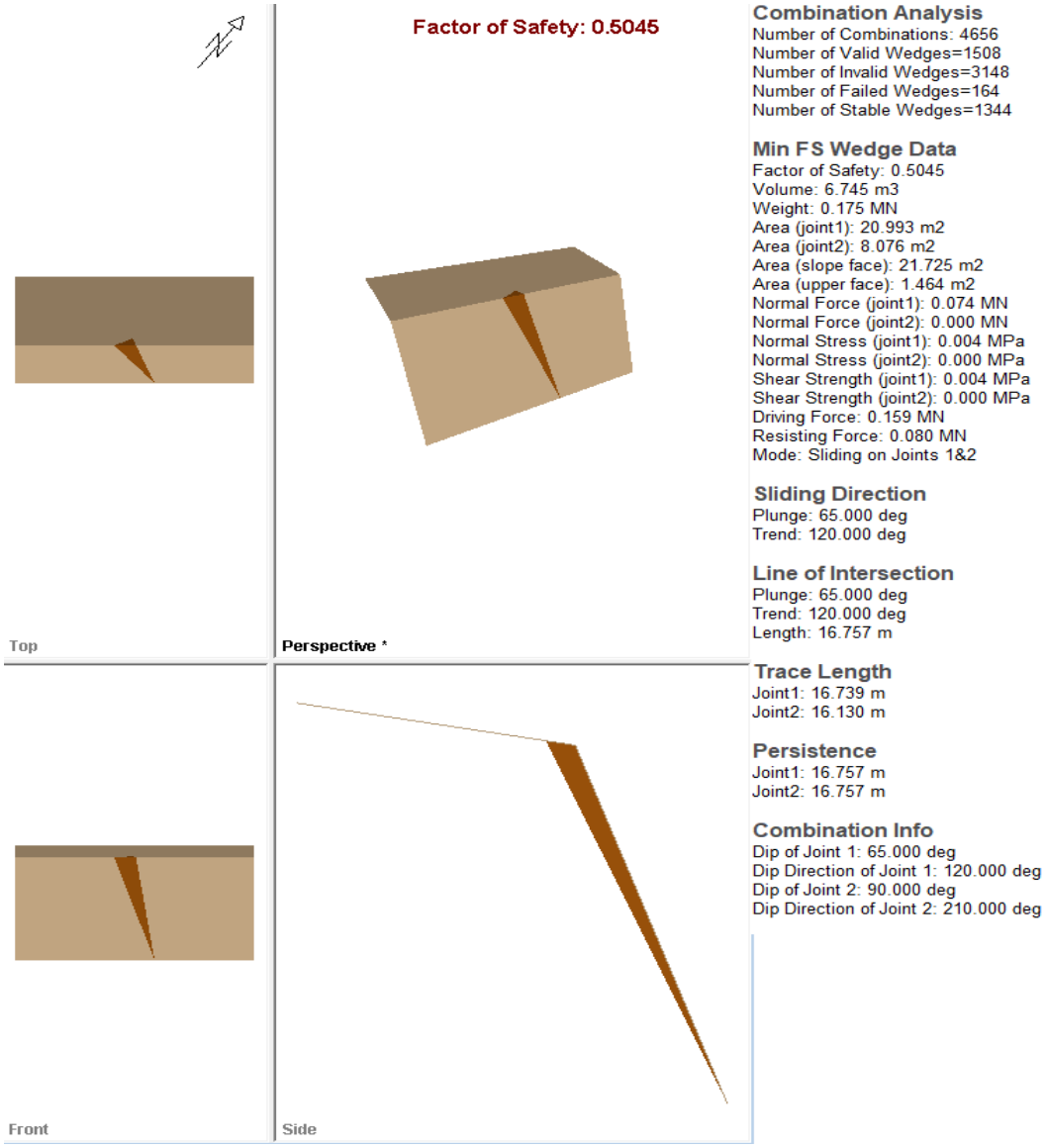

Figure 22: Combinations analysis of failing wedges performed in SWedge with a dip/dip direction of 70/143°.

When the slope dip is increased to 80° the most unstable wedge's factor of safety decreases to 0,29. 302 failed wedges from a total valid count of 1720 yields a probability of failure of 18,6% (fig 23).

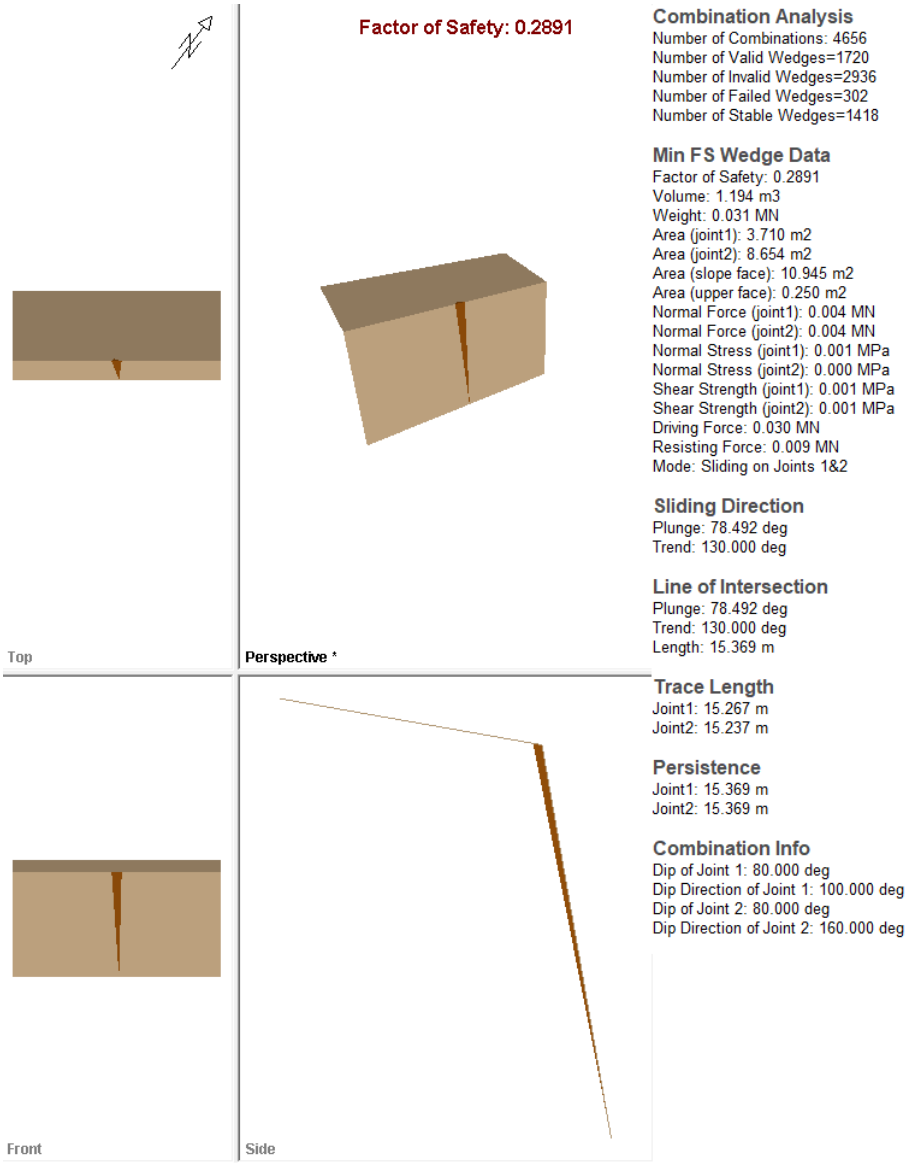

Figure 23: Combinations analysis of the northwest slope with a dip degree of 80°

The third scenario with a dip/dip direction of 90°/143° have a low factor of safety for the most unstable wedge of 0,10 with a total of 513 failed wedges from 1983 valid wedges. This result in a probability of failure of 25,9% (fig 24).

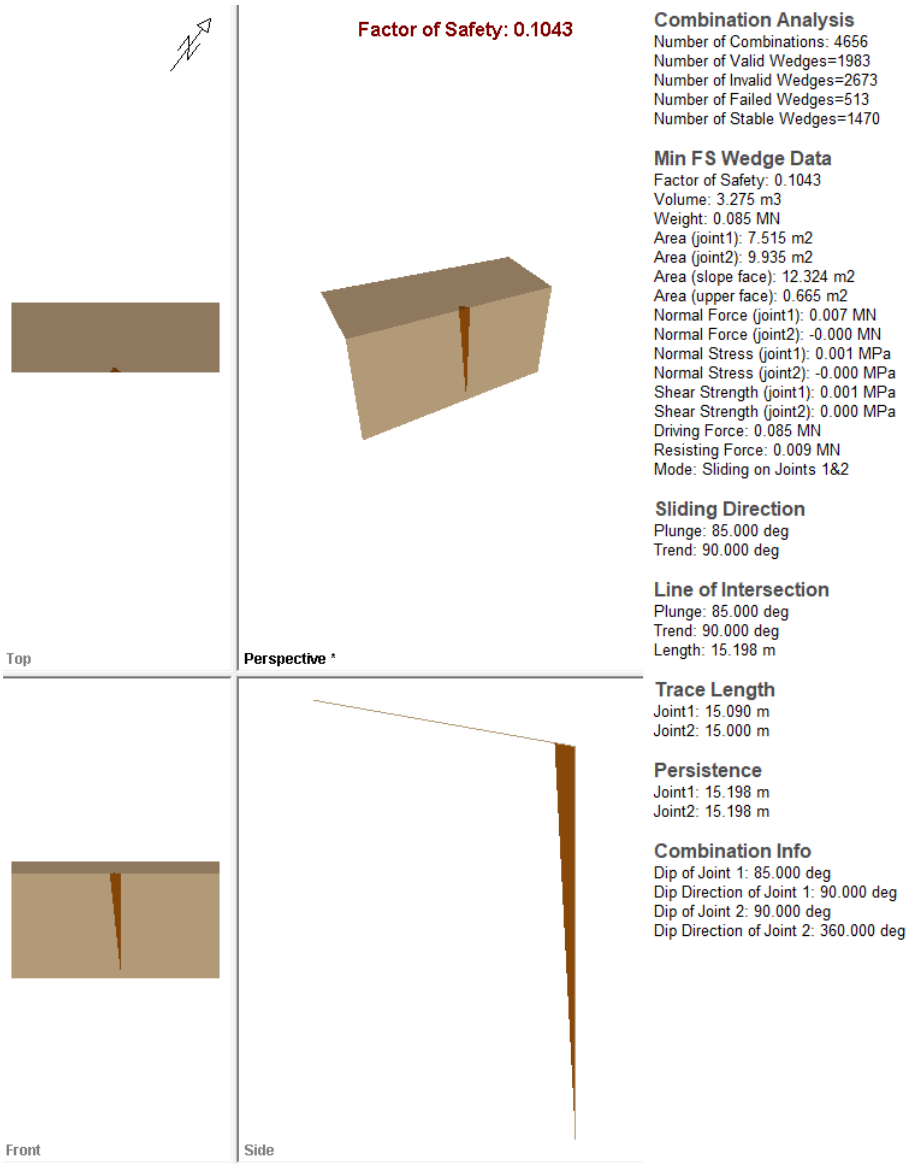

Figure 24: Combinations analysis performed in SWedge on the north-western slope with a dip/dip degree of 90/143°.

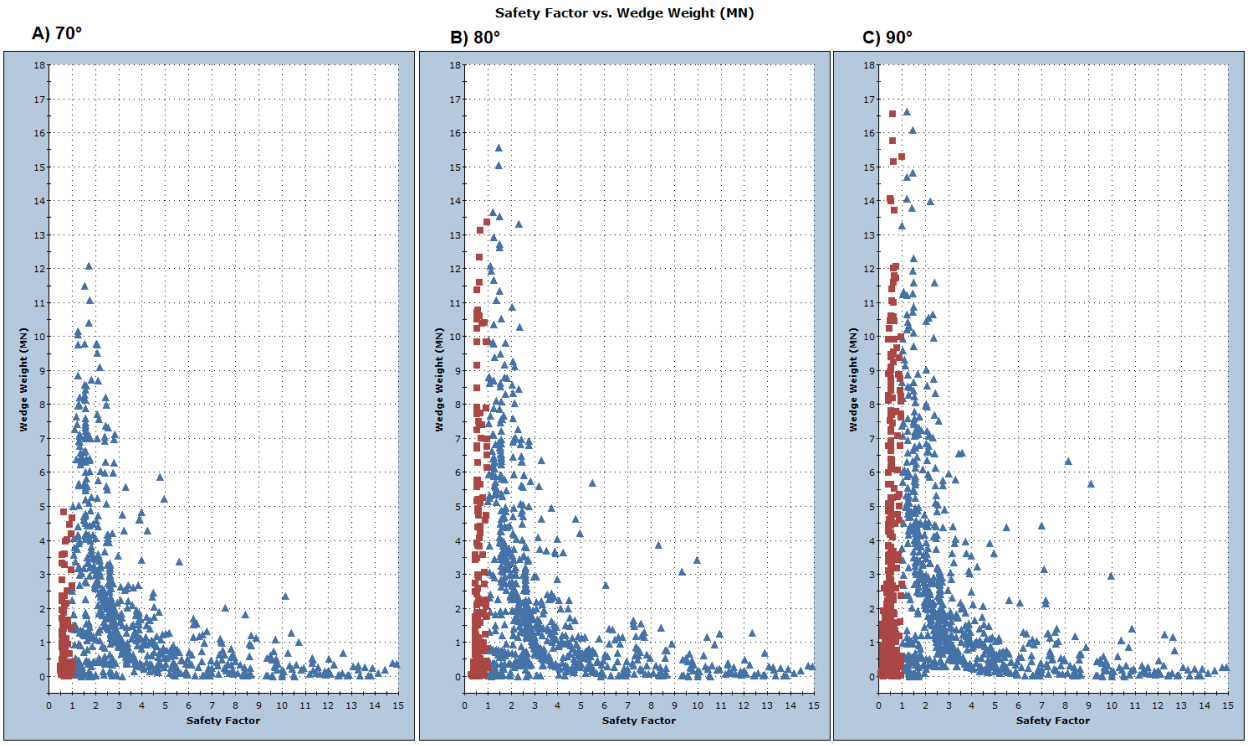

Figure 25: Scatter plots showing the increasing number of failed wedges on the north-western side of the railroad, additionally plots A, B and C show how the wedges increase in weight with a steeper dip angle.

When analysing the south-eastern side of the railroad similar observations were made. The first scenario with a dip degree of 70° generates a minimum factor of safety of 0,57, 150 failed wedges from a total of 1085 valid wedges. The probability of failure is 13,8% (fig 26).

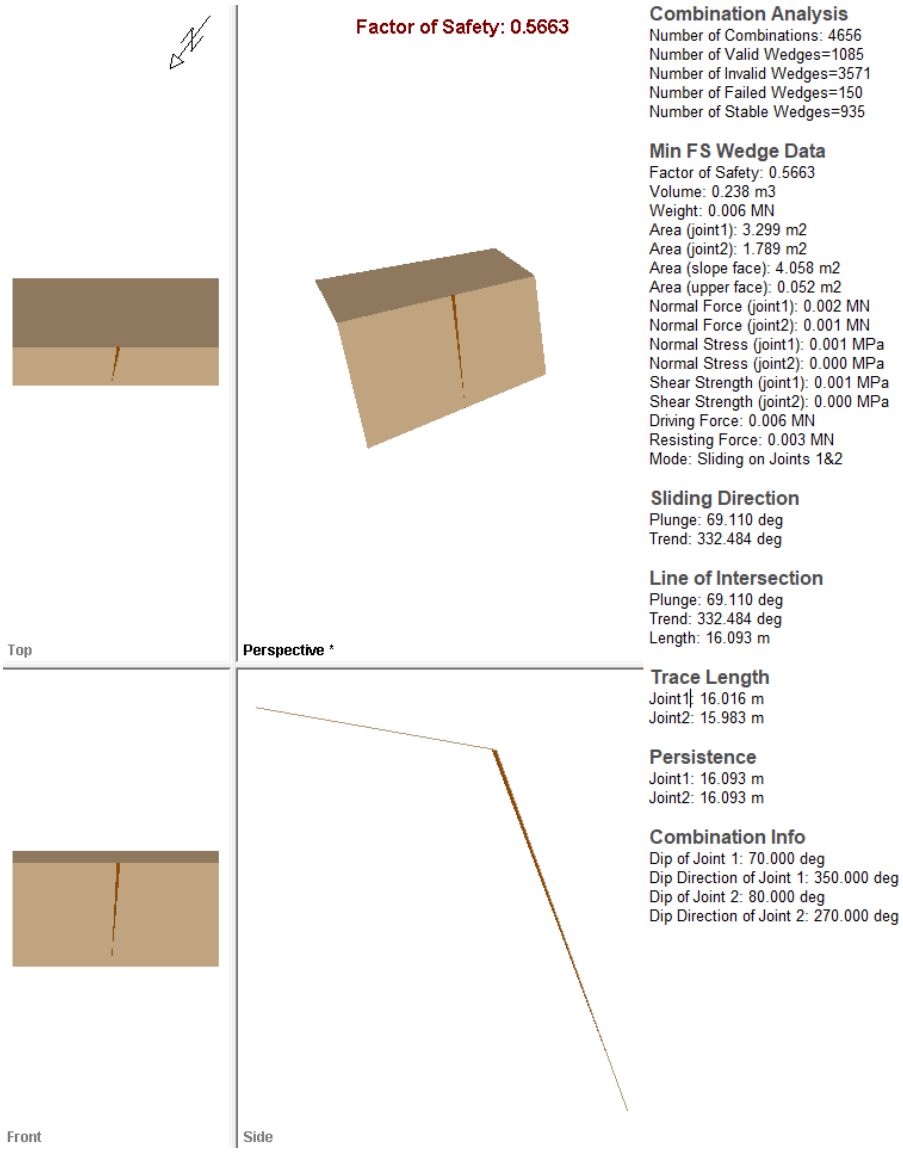

Figure 26: Combinations analysis of failing wedges performed in SWedge with a dip/dip direction of 70/323°.

When applying a dip/dip direction of 80°/323° the minimum factor of safety is 0,26. Probability of failure is calculated to 25,6% from 1361 valid wedges were 348 can fail (fig 27).

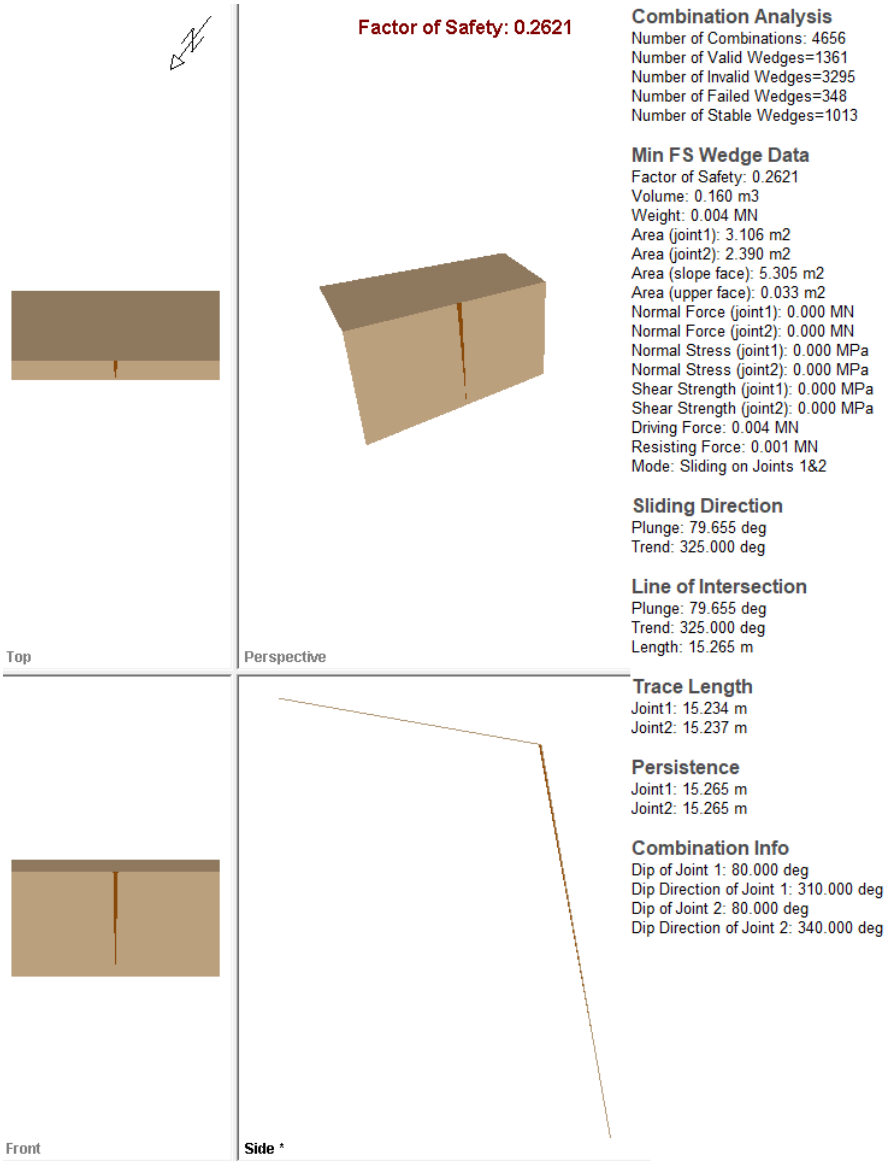

Figure 27: Combinations analysis of the northwest slope with a dip degree of 80°

The final case with a dip angle of 90° yields a factor of safety of 0,07 for the most unstable wedge. 1749 valid wedges with 718 failed wedges results with a probability of failure 41% (fig 28).

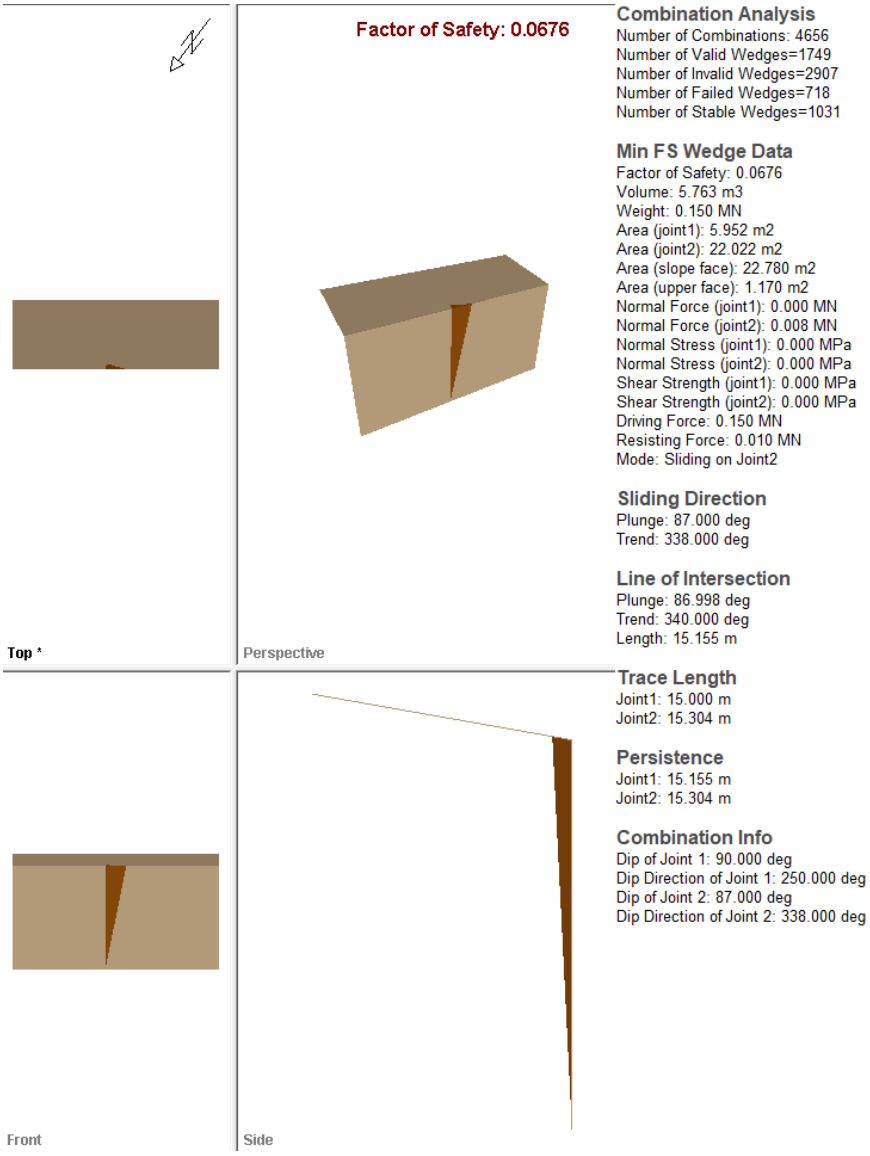

Figure 28: Combinations analysis performed in SWedge on the south-eastern slope with a dip/dip degree of 90/323°.

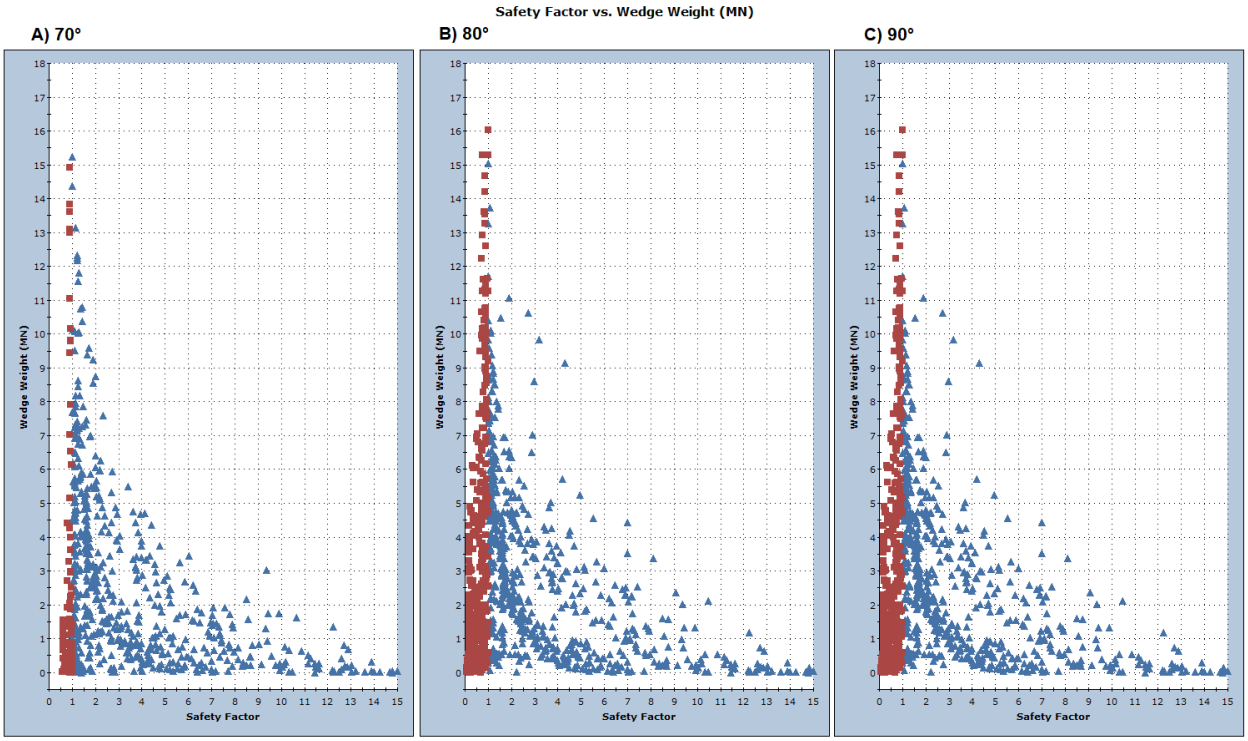

Figure 29: Scatter plots showing the increasing number of failed wedges on the south-eastern side of the railroad, additionally plots A, B and C show how the wedges increase in weight with a steeper dip angle.

6 Discussion

A complete slope design requires consideration of a large number of geological, geotechnical, groundwater and operational factors despite having all of these, a slope stability calculation should never be treated as an end in itself but rather as a contribution to the overall design process.

The planar sliding analysis show low to zero risk of sliding, both when using 19 measurements and when including 91 points. Hence, this mode of failure should not be considered a risk. An additional investigation of toppling failure was originally part of the plan of investigation but due to shortage of time this had to be cut in favour of a richer wedge analysis. Toppling could however, also have had an influence on the slope stability since there was in-dipping fractures present in the slope.

Since the analyses of the kinematic sensitivity showed that the main contributor to wedges failing is due to the degree of the slope dip, a more acute angle of dip would be desired to minimalize the risk of fallouts. On the other hand, by choosing a lesser incline more rock must be removed in the first place. By alternating the dip angle of the slope in different sections where the risk of failing seems more likely a method for the least amount of rock having to be shipped away can be reached.

The friction angle was a factor of importance when low values were applied (fig 18&19) to the model but several scientists among Marinos and Hoek (2000) suggest higher values for granodiorite and granite. In the case of Hamnbanan where the majority of the bedrock is made up of previous mentioned rock it is

safe to use a higher estimate, hence 30° is used in general throughout this paper which is also how it was performed in Trafikverkets initial investigation (Thorsager & Andersson, 2018).

6.1.1 Comparison of data sets

When comparing data sets it is obvious that some set of rules need to be in place for this to be viable. With some sets only containing one or few datapoints but other sets contain many points, some type of weighted system might be a good idea, with more datapoints within a certain set making it more of a risk factor. Right now, it is indicated the same way if there is one or ten poles within a set. Another thing worth considering is the distance between the poles when creating sets. In rocsience there are three different ways to define a set, either by creating a set window, drawing a set by freehand or creating a set from a cluster analysis. The first two options can be drawn as big or small as desired, there are no limits and for the cluster analysis a maximum angle for a cone is selected that will surround poles within the desired degree that was selected. Hence, depending on how the poles are divided into sets can control the outcome of the result and therefore a more intricate set of rules or guidelines for creating sets is desired. In figure 7c and 7d the exact same data set is used but depending on how sets are divided it result in quite different outcomes.

6.2 Sources of error

All strike and dip values obtained from the MUR from Trafikverket (appendix A) were numbers ending with either zero or five which strongly suggest that these are rounded numbers but no information about the rounding of numbers have been given in the document. Even if it just by a few degrees it still skews the result and several of these small corrections can lead to bigger consequences. Furthermore, there is an evaluation of the surveys in the MUR which reads that “all mappings are performed with ocular methods, which gives a certain spread in the result” (Trafikverket, 2018) and as mentioned in the quote this will further increase the uncertainty of the measurements.

The data that was used to create the stereonets was from a large area with only 19 out of the 91 data points from the direct area of interest. This inclusion of data points adds a third set of joints which would not be visible with the first 19 points. It is mentioned in the report from Trafikverket that the whole area is considered as one big block since the rock seem quite homogenous from an overview, but I have seen no further investigation of this.

Furthermore, groundwater pressure is neglected in this study. There were drillholes for measuring the water pressure in the rock within the whole area but there was no hole in the direct vicinity of the area of interest for me. Groundwater pressure is an important factor and as mentioned above, a complete slope design requires considerations of many parameters, groundwater is one of them.

Magnetic declination does not seem to have been a major contributor to the result. The magnetic declination in the Gothenburg area in 2013 was 2,7 degrees east of north and today, 2022, it is 4,3 degrees east of north. In either case the declination from the true north is so small it can be neglected.

7 Conclusion

It is always easier to judge something in hindsight but in the case of Hamnbanan I think it should have been possible to determine a more favourable slope design to minimize failed wedges. By constructing a slope that is not completely vertical but instead creating it with a lesser incline the total volume of fallouts could have been prevented (fig 25&29). This should at least have been considered in certain sections

where joints were an obvious problem and in the area of the shear zone. Furthermore, this report shows that the way data is collected and reported plays a major factor in the result and that it is important to make a big effort when collecting and recording data.

8 References

Hoek, E. (2009). Fundamentals of Slope Design. https://www.rocscience.com/assets/resources/learning/hoek/2009-Fundamentals-of-Slope-Design.pdf

Hoek, E., & Diederichs, M. S. (2006). Empirical estimation of rock mass modulus. *International Journal of Rock Mechanics and Mining Sciences*, *43*(2), 203-215. https://doi.org/https://doi.org/10.1016/j.ijrmms.2005.06.005

Karlsson, J. (2022). *Hamnbanan Göteborg*. https://www.bergab.se/hamnbanan-goteborg

Marinos, P., & Hoek, E. (2000). Gsi: A Geologically Friendly Tool For Rock Mass Strength Estimation. ISRM International Symposium,

Rocscience. (n.d.-a). *About the Company*. https://www.rocscience.com/about/company

Rocscience. (n.d.-b). *Feature Analysis*. https://www.rocscience.com/help/dips/tutorials/tutorials-overview/feature-analysis

Rocscience. (n.d.-c). *Kinematic Analysis (Planar Sliding)*. https://www.rocscience.com/help/dips/tutorials/tutorials-overview/kinematic-analysis-planar-sliding

Rocscience. (n.d.-d). *Kinematic Analysis (Wedge Sliding)*. https://www.rocscience.com/help/dips/tutorials/tutorials-overview/kinematic-analysis-wedge-sliding

Rocscience. (n.d.-e). *Overview - Technical Specifications Dips*. https://www.rocscience.com/help/dips/overview/technical-specifications

Rocscience. (n.d.-f). *Overview - Technical Specifications SWedge*. (https://www.rocscience.com/help/swedge/overview/technical-specifications)

Thorsager, P., & Andersson, T. (2018). *PM Bergteknik* (Hamnbanan Göteborg, dubbelspår Eriksberg-Pölsebo, Issue 0.1).

Trafikverket. (2018). *Markteknisk undersökningsrapport (MUR) Bergteknik* (Förfrågningsunderlag Totalentreprenad Hamnbanan Göteborg, dubbelspår Eriksberg-Skandiahamnen, Issue 7.1.3).

Trafikverket. (2022). *Västra GötalandHamnbanan Göteborg*. Retrieved March 24 from https://www.trafikverket.se/vara-projekt/projekt-i-vastra-gotalands-lan/hamnbanan-goteborg/#tidsplan

9 Appendix A:

Table 1: Data retrieved from the ground technical survey *(Markteknisk undersökningsrapport, MUR)* that have been translated from Swedish to English.

Subarea	Fracture	Rock	Colour	Fracture type	Strike (°)	Dip (°)	Fracture frequency (counts/m)	Fracture rawness (I-IX)	Jr (joint roughness number)	Ja (joint alteration number)	RQD (%)	Jn (joint set number)
Km 4+310 - 4+530 Km	1	Granodiorite phenocryst	Redgrey	Group	0	20	1-2	V	2		75-90	12
Km 4+310 - 4+530 Km	2	Granodiorite phenocryst	Redgrey	Group	0	20	1-2	V	2		75-90	12
Km 4+310 - 4+530 Km	3	Granodiorite phenocryst	Redgrey	Random	20	60	single	IV	3	1	90-100	12
Km 4+310 - 4+530 Km	4	Granite	Greyred	Group	40	20	0.5-1	V	2		90-100	12
Km 4+310 - 4+530 Km	5	Granite	Greyred	Random	50	40	single	VII	1,5	1	90-100	12
Km 4+310 - 4+530 Km	6	Granodiorite phenocryst	Redgrey	Group	100	65						12
Km 4+310 - 4+530 Km	7	Granite	Greyred	Group	100	80	<0.5	V	2			12
Km 4+310 - 4+530 Km	8	Granodiorite phenocryst	Redgrey	Group	100	90	0.5-2	IV	3	1	75-90	12
Km 4+310 - 4+530 Km	9	Granodiorite phenocryst	Redgrey	Group	100	90	single	V	2	1	90-100	12
Km 4+310 - 4+530 Km	10	Gneiss	Greyred	Fol.	150	70	single				90-100	12
Km 4+310 - 4+530 Km	11	Granodiorite phenocryst	Redgrey	Random	170	70	0.5-1	V	2		90-100	12
Km 4+310 - 4+530 Km	12	Granite	Redgrey	Random	190	50	0.5-1	V	2		90-100	12
Km 4+310 - 4+530 Km	13	Pegmatite	Red	Group	200	80	single				90-100	12
Km 4+310 - 4+530 Km	14	Granodiorite phenocryst	Redgrey	Group	200	85						12
Km 4+310 - 4+530 Km	15	Granodiorite phenocryst	Redgrey	Group	240	90	1-2	IV	3	1	75-90	12
Km 4+310 - 4+530 Km	16	Granite	Greyred	Group	280	80	<0.5	V	2	1	90-100	12
Km 4+310 - 4+530 Km	17	Gneiss	Greyred	Group	285	60	0.5-2	IV	3	1	75-90	12
Km 4+310 - 4+530	18	Granodiorite phenocryst	Redgrey	Group	290	80	0.5-2	IV	3	1	75-90	12

Subarea	Fracture	Rock	Colour	Fracture type	Strike (°)	Dip (°)	Fracture frequency (counts/m)	Fracture rawness (I-IX)	Jr (joint roughness number)	Ja (joint alteration number)	RQD (%)	Jn (joint set number)
Km 4+310 - 4+530	19	Granite	Greyred	Group	310	30	0.5-2	V	2		75-90	12
Km 4 +720 - 4+830	1	Granodiorite phenocryst	Redgrey	Group	0	20						12
Km 4 +720 - 4+830	2	Granodiorite phenocryst	Redgrey	Group	0	20						12
Km 4 +720 - 4+830	3	Granodiorite phenocryst	Redgrey	Group	0	20						12
Km 4 +720 - 4+830	4	Granodiorite phenocryst	Redgrey	Group	10	60						12
Km 4 +720 - 4+830	5	Granodiorite phenocryst	Redgrey	Random	30	65	0.5-1	VII	1,5		90-100	12
Km 4 +720 - 4+830	6	Granodiorite phenocryst	Redgrey	Group	90	70						12
Km 4 +720 - 4+830	7	Granodiorite phenocryst	Redgrey	Group	95	70	1-2	VII	1,5	1	75-90	12
Km 4 +720 - 4+830	8	Granodiorite phenocryst	Redgrey	Group	100	85	<0.5	V	2		90-100	12
Km 4 +720 - 4+830	9	Granodiorite phenocryst	Redgrey	Random	140	90	0.5-1	IV	3		90-100	12
Km 4 +720 - 4+830	10	Granodiorite phenocryst	Redgrey	Shear zone	160	60	5	V	2		50-75	12
Km 4 +720 - 4+830	11	Granodiorite phenocryst	Redgrey	Group	160	80	0.5-1	IV	3		90-100	12
Km 4 +720 - 4+830	12	Granodiorite phenocryst	Redgrey	Fol.	165	60	single				90-100	12
Km 4 +720 - 4+830	13	Gneiss	Greyred	Shear zone	170	40	0.5-1	IV	3	1	90-100	12
Km 4 +720 - 4+830	14	Gneiss	Greyred	Fol.	170	40	0.5-1	IV	3	1	90-100	12
Km 4 +720 - 4+830	15	Granodiorite phenocryst	Redgrey	Group	170	90						12
Km 4 +720 - 4+830	16	Granodiorite phenocryst	Redgrey	Group	170	90	0.5-1	IV	3		90-100	12
Km 4 +720 - 4+830	17	Granodiorite phenocryst	Redgrey	Group	180	90	<0.5	IV	3		90-100	12
Km 4 +720 - 4+830	18	Granodiorite phenocryst	Redgrey	Group	220	30	0.5-1	V	2		90-100	12
Km 4 +720 - 4+830	19	Granodiorite phenocryst	Redgrey	Random	240	90	0.5-1	V	2		90-100	12
Km 4 +720 - 4+830	20	Pegmatite (Quartz)	White	Random	250	45	0.5-1	IV	3		90-100	12

Subarea	Fracture	Rock	Colour	Fracture type	Strike (°)	Dip (°)	Fracture frequency (counts/m)	Fracture rawness (I-IX)	Jr (joint roughness number)	Ja (joint alteration number)	RQD (%)	Jn (joint set number)
Km 4 +720 - 4+830	21	Granodiorite phenocryst	Redgrey	Random	250	90	0.5-1	VIII	1		90-100	12
Km 4 +720 - 4+830	22	Granodiorite phenocryst	Redgrey	Random	250	90	0.5-1	IV	3		90-100	12
Km 4 +720 - 4+830	23	Granodiorite phenocryst	Redgrey	Group	260	70						12
Km 4 +720 - 4+830	24	Granodiorite phenocryst	Redgrey	Group	270	**80**	0.5-1	V	2		90-100	12
Km 4 +720 - 4+830	25	Granodiorite phenocryst	Redgrey	Random	320	70	0.5-1	V	2		90-100	12
Km 4 +720 - 4+830	26	Pegmatite (Quartz)	White	Group	360	30						12
Km 4 +720 - 4+830	27	Granodiorite phenocryst	Redgrey	Group	360	85	0,5	V	2		90-100	12
Km 5 + 060 - 5+ 300	1	Gneiss		Group	0	20	0.5-1	IV	3		90-100	12
Km 5 + 060 - 5+ 300	2	Granite		Group	0	20	0.5-1	IV	3		90-100	12
Km 5 + 060 - 5+ 300	3	Granodiorite phenocryst		Group	0	20	0.5-1	IV	3		90-100	12
Km 5 + 060 - 5+ 300	4	Granodiorite phenocryst		Group	0	20	0.5-1	IV	3		90-100	12
Km 5 + 060 - 5+ 300	5	Granodiorite phenocryst		Group	0	20						12
Km 5 + 060 - 5+ 300	6	Gneiss		Group	10	35	0.5-1	IV	3		90-100	12
Km 5 + 060 - 5+ 300	7	Pegmatite (Quartz)		Group	10	80						12
Km 5 + 060 - 5+ 300	8	Granodiorite phenocryst		Group	30	30	1	IV	3		90-100	12
Km 5 + 060 - 5+ 300	9	Granodiorite phenocryst		Random	40	60	<0.5	VIII	1		90-100	12
Km 5 + 060 - 5+ 300	10	Granodiorite phenocryst		Random	50	60	0.5-1	IV	3		90-100	12
Km 5 + 060 - 5+ 300	11	Granodiorite phenocryst		Group	110	80	0.5-1	VII	1,5		90-100	12
Km 5 + 060 - 5+ 300	12	Gneiss		Returning	120	90	0.5-1	IV	3		90-100	12
Km 5 + 060 - 5+ 300	13	Granodiorite phenocryst		Returning	120	90	0.5-1	V	2		90-100	12
Km 5 + 060 - 5+ 300	14	Granodiorite phenocryst		Returning	135	85	1-2	IV	3		75-90	12

Subarea	Fracture	Rock	Colour	Fracture type	Strike (°)	Dip (°)	Fracture frequency (counts/m)	Fracture rawness (I-IX)	Jr (joint roughness number)	Ja (joint alteration number)	RQD (%)	Jn (joint set number)
Km 5 + 060 - 5+ 300	15	Granodiorite phenocryst		Returning	140	90	0.5-1	VII	1,5		90-100	12
Km 5 + 060 - 5+ 300	16	Granodiorite phenocryst		Fol.	160	50						12
Km 5 + 060 - 5+ 300	17	Granite		Group	160	80	0.5-1	IV	3		90-100	12
Km 5 + 060 - 5+ 300	18	Granodiorite phenocryst		Group	160	90	0.5-1	IV	3		90-100	12
Km 5 + 060 - 5+ 300	19	Granodiorite phenocryst		Group	170	50	0.5-1	V	2		90-100	12
Km 5 + 060 - 5+ 300	20	Granite		Group	170	90	<0.5	IV	3		90-100	12
Km 5 + 060 - 5+ 300	21	Granite		Fol.	180	40	<0.5	V	2		90-100	12
Km 5 + 060 - 5+ 300	22	Granodiorite phenocryst		Random	190	45	<0.5	VII	1,5		90-100	12
Km 5 + 060 - 5+ 300	23	Granite		Random	220	40	<0.5	V	2		90-100	12
Km 5 + 060 - 5+ 300	24	Granite		Returning	220	80	0.5-1	IV	3		90-100	12
Km 5 + 060 - 5+ 300	25	Granodiorite phenocryst		Random	230	60		IV	3		90-100	12
Km 5 + 060 - 5+ 300	26	Granodiorite phenocryst		Returning	240	90	0.5-1	IV	3		90-100	12
Km 5 + 060 - 5+ 300	27	Granodiorite phenocryst		Returning	250	80	0.5-1	VII	1,5		90-100	12
Km 5 + 060 - 5+ 300	28	Granodiorite phenocryst		Group	260	85	single				90-100	12
Km 5 + 060 - 5+ 300	29	Granodiorite phenocryst		Group	270	90	single				90-100	12
Km 5 + 060 - 5+ 300	30	Granite		Random	290	70	<0.5	IV	3		90-100	12
Km 5 + 060 - 5+ 300	31	Granodiorite phenocryst		Random	300	80	0.5-1	V	2		90-100	12
Km 5 + 060 - 5+ 300	32	Granodiorite phenocryst		Random	320	60	0.5-1	VII	1,5		90-100	12
Km 5 + 060 - 5+ 300	33	Granodiorite phenocryst		Returning	340	70	0.5-1	VII	1,5		90-100	12
Km 5 + 060 - 5+ 300	34	Granodiorite phenocryst		Group	350	30	0.5-1	V	2		90-100	12
Km 5 + 060 - 5+ 300	35	Granite		Returning	355	55	<0.5	IV	3		90-100	12

Subarea	Fracture	Rock	Colour	Fracture type	Strike (°)	Dip (°)	Fracture frequency (counts/m)	Fracture rawness (I-IX)	Jr (joint roughness number)	Ja (joint alteration number)	RQD (%)	Jn (joint set number)
Km 5 + 060 - 5+ 300	36	Gneiss		Returning	360	40	<0.5	V	2		90-100	12
Km 5 +790 - 6+320	1	Gneiss		Group	0	20	0.5-1	IV	3		90-100	6
Km 5 +790 - 6+320	2	Gneiss		Group	70	80		IV	3			6
Km 5 +790 - 6+320	3	Metabasalt		Group	100	20	0.5-1	IV	3		90-100	6
Km 5 +790 - 6+320	4	Gneiss		Random	130	80	0.5-1	IV	3		90-100	6
Km 5 +790 - 6+320	5	Gneiss		Fol.	180	40	0.5-2	V	2		90-100	6
Km 5 +790 - 6+320	6	Gneiss		Group	180	80	0.5-1	IV	3		75-90	6
Km 5 +790 - 6+320	7	Metabasalt		Group	180	90	0.5-1	IV	3		90-100	6
Km 5 +790 - 6+320	8	Gneiss		Group	240	80	<0.5	IV	3	1	90-100	6
Km 5 +790 - 6+320	9	Granite		Group	260	90	single	IV	3	0,75	90-100	6